Title
Dopamine dysregulation in a mouse model of paroxysmal nonkinesigenic dyskinesia

Journal
JOURNAL OF CLINICAL INVESTIGATION, 122(2)

ISSN
0021-9738

Authors
Lee, Hsien-yang
Nakayama, Junko
Xu, Ying
et al.

Publication Date
2012

DOI
10.1172/JCI58470

Peer reviewed

Dopamine dysregulation in a mouse model of paroxysmal nonkinesigenic dyskinesia

Hsien-yang Lee,[1] Junko Nakayama,[1] Ying Xu,[1] Xueliang Fan,[2] Maha Karouani,[3] Yiguo Shen,[1] Emmanuel N. Pothos,[3] Ellen J. Hess,[2] Ying-Hui Fu,[1] Robert H. Edwards,[1] and Louis J. Ptácek[1,4]

[1]Department of Neurology, UCSF, San Francisco, California, USA. [2]Department of Pharmacology, Emory University School of Medicine, Atlanta, Georgia, USA. [3]Department of Molecular Physiology and Pharmacology and Program in Neuroscience, Tufts University School of Medicine, Boston, Massachusetts, USA. [4]Howard Hughes Medical Institute, UCSF, San Francisco, California, USA.

Paroxysmal nonkinesigenic dyskinesia (PNKD) is an autosomal dominant episodic movement disorder. Patients have episodes that last 1 to 4 hours and are precipitated by alcohol, coffee, and stress. Previous research has shown that mutations in an uncharacterized gene on chromosome 2q33–q35 (which is termed *PNKD*) are responsible for PNKD. Here, we report the generation of antibodies specific for the PNKD protein and show that it is widely expressed in the mouse brain, exclusively in neurons. One PNKD isoform is a membrane-associated protein. Transgenic mice carrying mutations in the mouse *Pnkd* locus equivalent to those found in patients with PNKD recapitulated the human PNKD phenotype. Staining for c-fos demonstrated that administration of alcohol or caffeine induced neuronal activity in the basal ganglia in these mice. They also showed nigrostriatal neurotransmission deficits that were manifested by reduced extracellular dopamine levels in the striatum and a proportional increase of dopamine release in response to caffeine and ethanol treatment. These findings support the hypothesis that the PNKD protein functions to modulate striatal neurotransmitter release in response to stress and other precipitating factors.

Introduction

The paroxysmal dyskinesias consist of clinically and genetically distinct phenotypes, including paroxysmal kinesigenic dyskinesia, paroxysmal exercise-induced dyskinesia, and paroxysmal nonkinesigenic dyskinesia (PNKD) (1, 2). PNKD is a highly penetrant autosomal dominant disorder in which individuals have 1- to 4-hour attacks consisting of dystonia and choreoathetosis (3). These attacks can be induced reliably by administration of caffeine or alcohol and frequently when patients are stressed. The causative gene was mapped to chromosome 2q33–q35 (4, 5), and mutations in the *PNKD* gene (formerly called *MR-1*) were subsequently identified in PNKD families (6–10).

The *PNKD* gene has at least 3 alternate splice forms, which encode proteins of 385, 361, and 142 amino acids. The long isoform of PNKD (PNKD-L) is specifically expressed in CNS, while the medium isoform (PNKD-M) and short isoform (PNKD-S) are ubiquitously expressed (7). Two missense mutations (Ala to Val) located at amino acids 7 or 9 of PNKD-L and PNKD-S were found in most patients, and a third mutation (Ala to Pro) at position 33 was reported in 1 family (11). Both PNKD-L and PNKD-M have a putative catalytic domain that is homologous to hydroxyacylglutathione hydrolase (HAGH), a member of the zinc metallo-hydrolase enzyme family, which contains β-lactamase domains. HAGH functions in a pathway to detoxify methylglyoxal, a by-product of oxidative stress (12). The normal role of PNKD in cells and the contribution of mutations to pathophysiology of PNKD are not known.

Dyskinesia is seen with many genetic and acquired disorders of the brain. Theoretically, such hyperkinetic movements could have their genesis in the basal ganglia, the cerebellum, or even in the cortex. Having cloned the gene and shown by in situ hybridization that it is widely expressed, we were interested in probing the pathophysiology of this fascinating disorder.

In this study, we generated polyclonal antibodies specific for detecting PNKD isoforms. We also generated WT and mutant *Pnkd*-transgenic and *Pnkd*-KO mice in order to determine whether they can recapitulate human PNKD phenotypes. Together, these reagents provided a unique opportunity to begin addressing questions regarding the pathophysiology of PNKD. We specifically began by determining the expression pattern of the *Pnkd* gene and protein. Next, we set out to see whether attacks in mice could be precipitated by the same stimuli that cause attacks in human PNKD patients. Since alcohol and caffeine are known to be "dirty" drugs that act on many receptor systems in the brain, targeted neuropharmacological agents were used to test specific pathways through which they might be acting. Finally, the neurotransmitter systems and receptors involved in transducing the abnormal dyskinetic movements in PNKD and the brain region or regions involved were also investigated. Thus, these studies were aimed at a more systems-level understanding of the pathophysiology as opposed to the molecular or cellular basis of PNKD. Such understanding, along with more work aimed at the molecular basis of PNKD, will be necessary to ultimately develop better therapies for paroxysmal dyskinesias and, potentially, other movement disorders.

Results

Nomenclature. In this study, standard nomenclature for names of genes and proteins was used. In vitro experiments were performed in cells transfected with the human cDNA, and in vivo experiments were done in mice. *PNKD* represents the human gene name, while PNKD is the human protein name and the acronym for the disorder paroxysmal nonkinesigenic dyskinesia. *Pnkd* is the mouse gene name, and Pnkd is the name for the mouse protein. "Pnkd mice" is used to denote the animal model we created that harbored the PNKD phenotype (i.e., mice transgenic for a BAC harboring both the A7V- and A9V-encoding *Pnkd* mutations).

Conflict of interest: The authors have declared that no conflict of interest exists.
Citation for this article: *J Clin Invest.* 2012;122(2):507–518. doi:10.1172/JCI58470.

Mapping Pnkd expression. In situ hybridization analysis previously showed that *Pnkd-L* mRNA is widely expressed in neurons of the CNS, but not in other tissues (7). We developed antibodies induced by oligopeptides from the N terminus (N-terminal antibody, expected to detect PNKD-L and -S) or C terminus (C-terminal antibody, expected to detect PNKD-M and -L) (Figure 1A). The C-terminal antibody detected 2 main bands (PNKD-L, ~47 kDa; PNKD-M, ~40 kDa), and the N-terminal antibody detected 2 bands (PNKD-L and PNKD-S, ~18 kDa) in mouse brain extracts (Figure 1B). We also tested the PNKD antibodies by detecting different isoforms of *PNKD-EGFP* transfected in human embryonic kidney 293 (HEK293) cells. In this heterologous expression system, the size of PNKD-L–EGFP, PNKD-M–EGFP, and PNKD-S–EGFP are approximately 75 kDa, approximately 70 kDA, and approximately 44 kDa, respectively (Supplemental Figure 1; supplemental material available online with this article; doi:10.1172/JCI58470DS1).

Immunohistochemistry using these antibodies confirmed that Pnkd is expressed widely in the CNS, including striatum, substantia nigra, cerebellum, and spinal cord (Figure 1, C–F). Pnkd is expressed both in striatal medium spiny neurons and in interneurons (Figure 1C) and also in substantia nigra pars compacta (SNC), which is constituted by dopaminergic neurons projecting to striatum, and substantia nigra pars reticulata (SNR), which is the output structure of the basal ganglia (Supplemental Figure 2A). In cerebellum, Pnkd is expressed in the granule cell and molecular layers and in Purkinje cells (Supplemental Figure 2B). Double immunochemical staining was performed with these antisera and markers specific for neurons or glia, and the results showed that Pnkd is expressed in neurons but not in oligodendrocytes or astrocytes (Figure 1, D–F). No difference in protein distribution was noted in *Pnkd* mutant mice versus littermate controls or *Pnkd* WT transgenic mice (data not shown).

There is one weak transmembrane segment prediction in PNKD-L (7). To determine whether PNKD-L is a transmembrane protein, we performed studies with permeabilized and nonpermeabilized *PNKD-L–EGFP*–transfected HEK293 cells. PNKD-L can be detected by both N- and C-terminal antibodies at the membrane in permeabilized cells, but not in nonpermeabilized cells (Figure 2A). We also prepared subcellular membrane fractions of HEK293 cells transfected with *PNKD-L–EGFP*, performed detergent partitioning with Triton X-114 (TX-114) onto subcellular membrane fractions, and showed that after TX-114 treatment, PNKD-L–EGFP can be detected in the hydrophilic layer, but not in the hydrophobic layer, using PNKD antibodies (Figure 2B). Thus, PNKD-L appears to be membrane associated, though not a transmembrane protein integral to the membrane.

A mouse model harboring the PNKD mutations recapitulates the PNKD phenotype. Three lines of *Pnkd* mutant BAC transgenic mice (mut-Tg, Pnkd mice) were generated by introducing both A7V- and A9V-encoding mutations into *Pnkd* (Figure 3A). The resulting BAC construct included the murine promoter and a large flanking region (extending 62 kb upstream) and was expected to contain all of the cis-acting regulatory elements needed to recapitulate the expression pattern of the endogenous loci. In addition, we generated *Pnkd* WT BAC transgenic mice (WT-Tg). Copy numbers of all lines were assessed by Southern blot; mut-Tg lines contained 1–2 copies, and the WT-Tg lines contained 2–3 copies (Figure 3B). Western blotting of mut-Tg and WT-Tg brain extracts showed that protein levels were consistent with the transgene copy number (Figure 3C). We also generated 2 lines of *Pnkd*-KO mice (Figure 3D). Both RT-PCR and Western blotting confirmed that they were true *Pnkd* nulls (Figure 3, E and F).

Multiple lines of mut-Tg, WT-Tg, and KO mice were observed, and all were fertile, with normal growth, and had no gross phenotypic abnormalities. None of the lines showed neuropathological defects by Nissl staining (data not shown). The body weight of PNKD mice trended lower than that of WT littermates, but the difference was not statistically significant. However, in mut-Tg mice, we observed dyskinesia after stress, such as prolonged handling (>15–30 minutes; see Supplemental Video 1). The dyskinesias included oral-facial movements (e.g., tongue protrusions) and stereotypic movements (repetitive sniffing and rearing in one location; see Supplemental Video 1). Dyskinesias were not seen in WT littermates, WT-Tg mice, or *Pnkd*-KO mice.

Mice were challenged with i.p. injection of caffeine (25 mg/kg) or ethanol (1.5 g/kg, 20% v/v). In mut-Tg mice, caffeine induced dyskinetic attacks approximately 10–15 minutes after treatment that persisted for 2 hours (Figure 4A and Supplemental Video 2). The severity of attacks in mut-Tg mice was significantly increased compared with that in predrug control or postdrug control using vehicle (saline, 10 ml/kg; Figure 4B). Behavioral effects of caffeine injection in WT littermates and WT-Tg mice were moderate hyperlocomotion during the first hour, but no dyskinesias were observed (Figure 4A). Ethanol also induced dyskinetic attacks in the mut-Tg mice (but not in WT littermates) beginning 10 minutes after injection and lasting 2–4 hours, and the attacks were more severe than those induced by caffeine. The mut-Tg mice suffered severe axial stiffness, with some abnormal movements of the limbs (Figure 4C and Supplemental Video 3, A and B). We did not observe any abnormal movements in the WT-Tg or KO mice after injection of caffeine or ethanol (data not shown). We examined multiple lines of mut-Tg, WT-Tg, and KO mice for i.p. injection of caffeine or ethanol, and the results showed no differences among genotypes. Unlike in dt^{sz} hamsters, there were no obvious age-dependent differences in the expression of dyskinesias of mut-Tg mice.

Neuroanatomical characterization of Pnkd mice. Since *Pnkd* is widely expressed in brain, we performed immunohistochemical studies with anti–c-Fos antibody to identify neuronal populations activated during PNKD attacks. Under basal conditions, almost no c-Fos–reactive cells were found in the brains of mut-Tg mice or WT littermates. Induction of c-Fos was seen in globus pallidus, subthalamic nucleus, and substantia nigra reticulata of mut-Tg mice, but not WT littermates, after caffeine injection (Supplemental Figure 3A). Similar patterns of c-Fos–positive signal were also seen in mutant mice after an attack was provoked with ethanol (data not shown). Minimal c-Fos–positive immunostaining was seen in cortical areas, but was not different in mut-Tg mice versus littermates. There were no obvious changes of c-Fos expression in basal ganglia or other brain regions in either WT-Tg or KO mice (data not shown). Thus, basal ganglia neurons are activated specifically in mut-Tg mice after induction of attacks.

Neurochemical studies show alteration of striatal dopamine signaling system of PNKD mice. Dopamine plays an important role in modulation of cortical and thalamic glutamatergic signal processing in the striatum, thus regulating movement (13–15). Therefore, we measured dopamine and its metabolites in the striatum by HPLC both before and after stimulating attacks. Pnkd and control mice had similar dopamine levels in striatum at rest (Figure 3D). After i.p. injection of caffeine (25 mg/kg), Pnkd mice had significantly higher levels of the dopamine metabolite 3,4-dihydroxyphenylacetic acid (DOPAC) and higher DOPAC/dopamine ratios than untreated animals ($P < 0.01$,

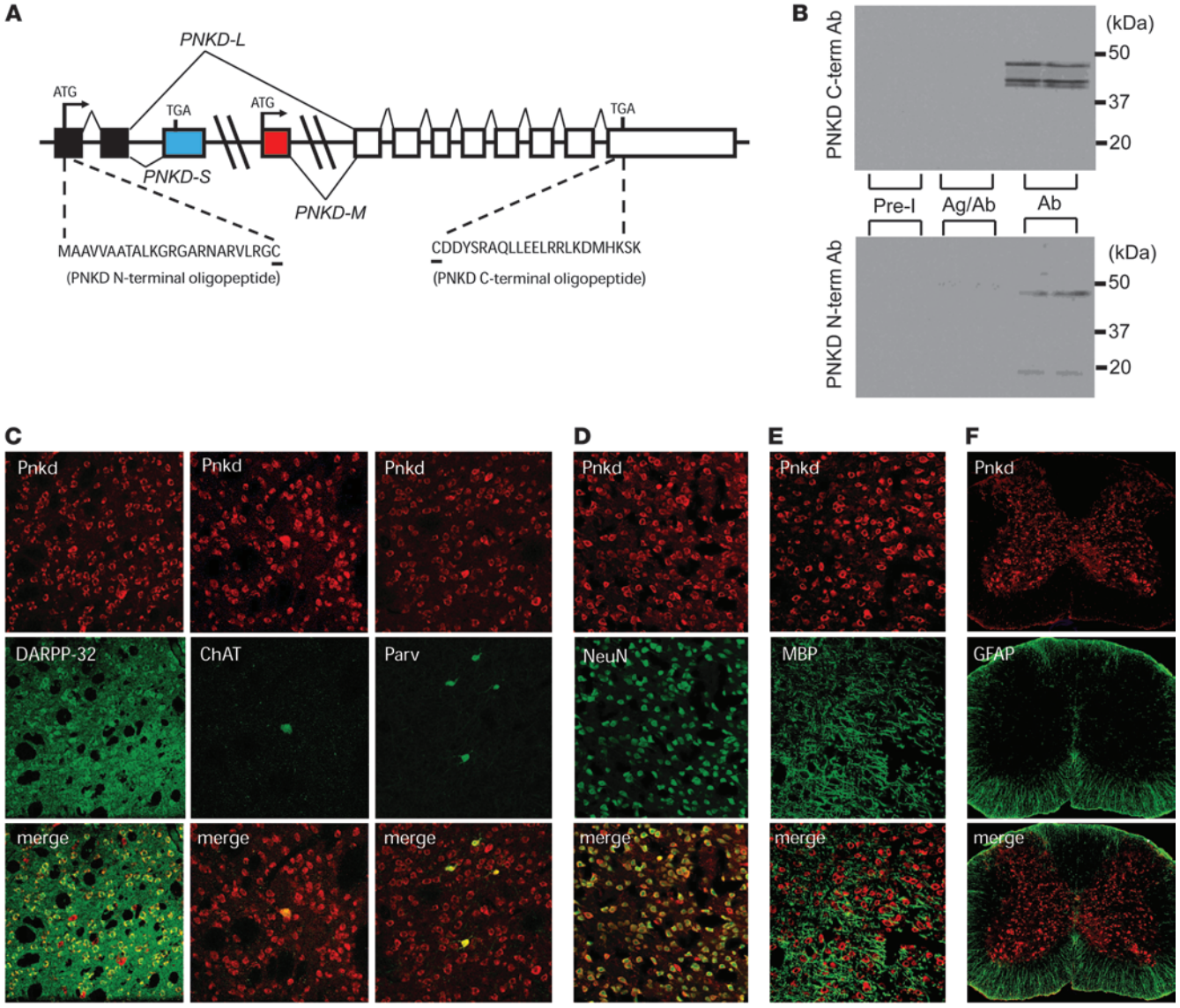

Figure 1

Pnkd immunochemistry in mouse brain. (**A**) Oligopeptides used to produce PNKD antibodies. Black rectangles represent exons shared by PNKD-L and PNKD-S; white rectangles represent exons shared by PNKD-L and PNKD-M; red rectangle represents the unique exon 1 of PNKD-M; blue rectangle represents the unique exon 3 of PNKD-S. Cysteines (underlined) were introduced in both oligopeptides to improve the coupling process. (**B**) Whole brain extracts on Western blots. The C-terminal antibody (1:5000 dilution) detected bands representing Pnkd-L (~47 kDa) and Pnkd-M (~40 kDa). The N-terminal antibody (1:500 dilution) detected bands representing Pnkd-L and Pnkd-S (~18 kDa). Pre-I, blots incubated with preimmune sera; Ag/Ab, PNKD antisera incubated with the oligopeptide against which they were raised; Ab, C- or N-terminal antisera only. (**C**) Double labeling in mice striatum with PNKD antibodies and either DARPP-32 (medium spiny neurons), ChAT (for cholinergic interneurons), or parvalbumin (Parv) (for GABAergic interneurons). (**D**) In striatum, Pnkd colocalizes with NeuN, a neuron-specific marker. (**E**) In striatum, Pnkd did not colocalize with oligodendrocyte-specific marker MBP. (**F**) Spinal cord cross section. Pnkd did not colocalize with astrocyte-specific marker GFAP. Original magnification, ×400.

Figure 4, E and F) or WT littermates treated with caffeine ($P < 0.05$ for DOPAC, Figure 4E; $P < 0.01$ for DOPAC/dopamine ratio; Figure 4F). The DOPAC levels and the DOPAC/dopamine ratio were significantly decreased in *Pnkd*-KO mice after injection of caffeine ($P < 0.01$) or ethanol (data not shown), but did not change in WT-Tg mice (Figure 4, E and F). Homovanillic acid (HVA), the terminal metabolite of dopamine metabolism, was also significantly increased in Pnkd mice after caffeine stimulation ($P < 0.05$; Figure 4G), while the levels of serotonin (5-HT) and its metabolized product (5-hydroxyindoleacetic acid [5-HIAA]) were not different in Pnkd versus control or before versus after caffeine challenge (Supplemental Figure 3, B and C). No obvious changes of DOPAC, DOPAC/dopamine ratio, and HVA levels were found in the *Pnkd* WT-Tg mice (Figure 4, D–G). Thus, dysfunction of dopamine signaling is associated with PNKD pathophysiology. Since the striatum is the primary basal ganglia region receiving dopaminergic and glutamatergic inputs from other brain

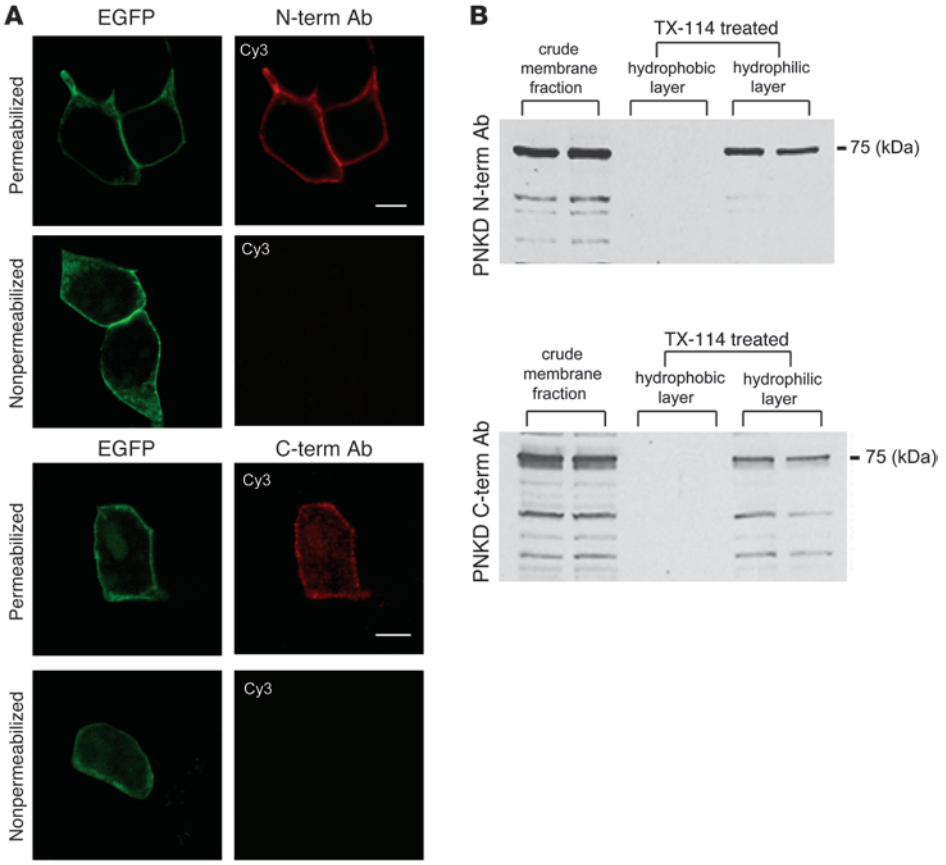

Figure 2
PNKD-L is a membrane-associated protein. (**A**) Immunostaining studies of permeabilized and nonpermeabilized HEK293 cells indicate that PNKD-L is a membrane-associated protein. HEK293 cells are transfected with *PNKD-EGFP* followed by immunohistochemical staining using N- and C-terminal PNKD antibodies and Cy3-conjugated goat anti-rabbit IgG secondary antibody. Both PNKD N- and C-terminal antibodies detect transfected PNKD-L–EGFP in permeabilized HEK cells, but fail to detect it in nonpermeabilized HEK cells. Scale bars: 10 microns. (**B**) Detergent phase partitioning of HEK293 membrane fraction transfected with *PNKD-L–EGFP*. The PNKD-L–EGFP (~75 kDa) can be detected in crude membrane fraction by both PNKD antibodies, but after TX-114 treatment, the PNKD-L–EGFP can be detected in the hydrophilic layer, but not in the hydrophobic layer.

structures (16–18), it is possible that expression of proteins involved in dopamine, glutamate, and/or adenosine signaling is altered in PNKD. To test this, striatal extracts from Pnkd and control mice were run on Western blots and probed with antibodies to proteins important for striatal function.

Because striatal dopamine signaling in Pnkd mice is altered (Figure 4, E–G), we examined the expression levels of proteins involved in dopamine synthesis, signaling, reuptake, and metabolism. Tyrosine hydroxylase (TH), the rate-limiting enzyme in the generation of dopamine, was no different for Pnkd mice versus controls (Supplemental Figure 4A). But D_1AR and D_2R were both significantly upregulated in the striata of Pnkd mice ($P < 0.05$; Supplemental Figure 4, B and C). We noted a trend (although not statistically significant) of decreased expression of vesicular monoamine transporter 2 (VMAT2) in PNKD striata versus control (Supplemental Figure 4D). Dopamine transporter (DAT) (~55 kDa in size) expression was significantly higher in the Pnkd mice compared with WT littermates ($P < 0.05$; Supplemental Figure 4E), and Pnkd mice also showed significantly higher expression of another main band of DAT in Western blots (~85 kDa, data not shown). There were no obvious differences in the expression of soluble catechol-methyltransferase (S-COMT) or membrane-bound COMT (MB-COMT) (19) in Pnkd mice versus littermate controls (Supplemental Figure 4F). Immunoblotting did not reveal any changes in expression levels of monoamine oxidase A (MAO-A) among genotypes (Supplemental Figure 4G). However, the level of MAO-B expression was significantly higher in Pnkd mice compared with littermate controls ($P < 0.05$; Supplemental Figure 4H).

We also examined striatal levels of synaptic vesicle proteins Rab3a, synapsin-1, and synaptophysin. Expression of these proteins was not altered in mutant versus control mice (Supplemental Figure 5, A–C). We also examined striatal proteins involved in GABA synthesis and glutamate reuptake (GAD65 and GAD67, EAAT3, and VGLUT1) by Western blotting. Expression of these proteins was no different in Pnkd versus control mice (Supplemental Figure 5, D–G) suggesting that GABA synthesis in striatum and glutamate reuptake are normal in Pnkd mice. We next examined expression of adenosine A_1 and adenosine A_{2A} receptors (A_1R and A_{2A}R), and adenosine kinase (ADK), a key regulator of adenosine metabolism. These were all unchanged in Pnkd mice versus WT littermates (Supplemental Figure 5, H–J). These results indicate that the alteration of striatal dopamine signaling system of Pnkd mice may contribute to dyskinetic attacks of Pnkd mice.

Pnkd mice have lower striatal dopamine release at rest, but an increased percentage of striatal dopamine release in response to challenges. To examine the pattern of nigrostriatal dopamine release, we performed in vivo microdialysis in alert, freely moving mice. Basal extracellular dopamine concentrations were assessed using the no net flux method to provide an unbiased estimate of transmitter concentration. The extracellular concentration of dopamine in Pnkd mice was less than 40% of that of control mice under basal conditions ($P < 0.05$; Figure 5A). In contrast, the extraction fraction was comparable in control and Pnkd mice, suggesting that the reduction in the basal extracellular dopamine concentrations in mutant mice is attributable to abnormalities in transmitter release (Figure 5B). Next, response

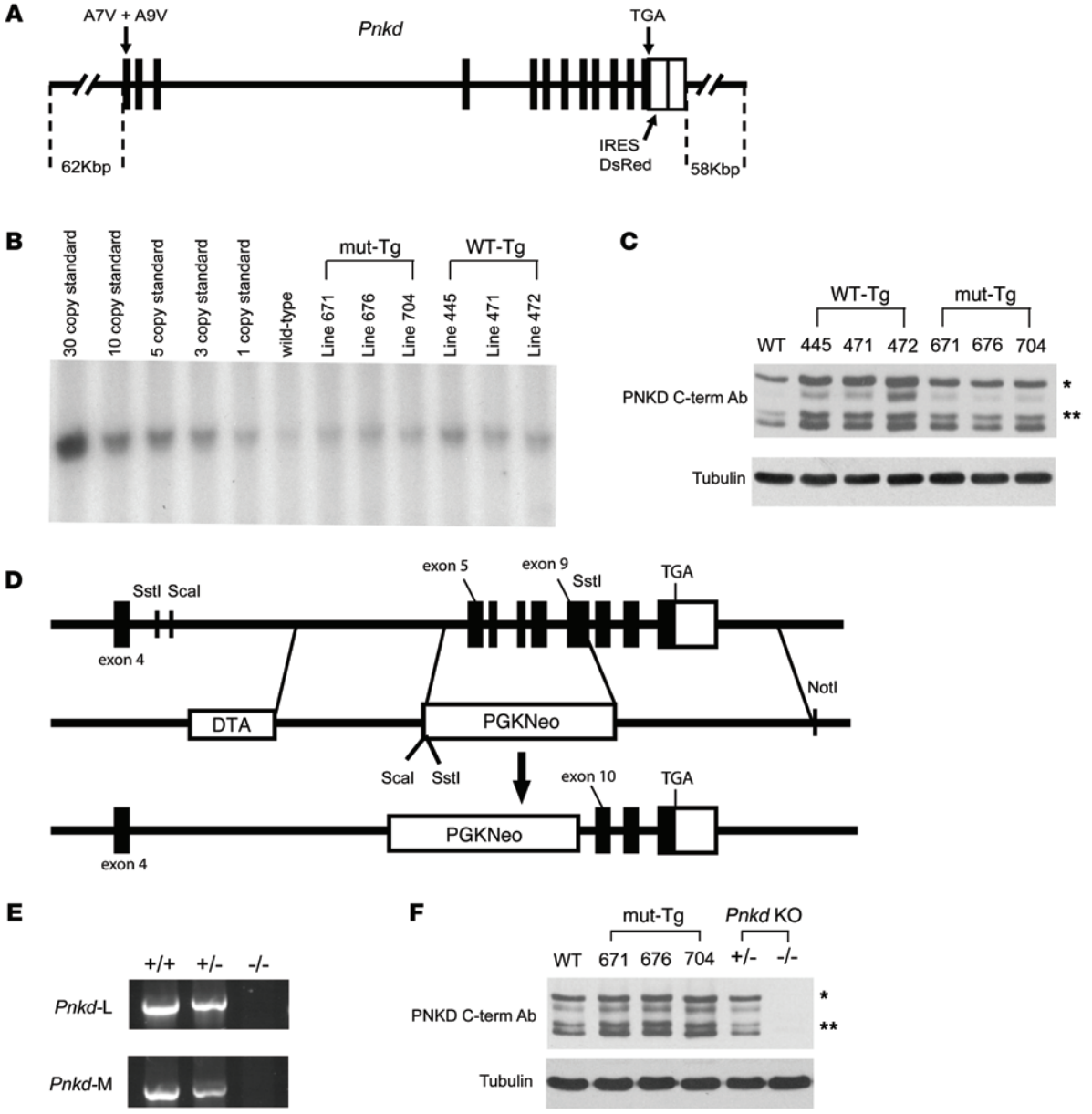

Figure 3

Generation of *Pnkd*-transgenic and -KO mice. (**A**) 2 human mutations (A7V and A9V) were introduced into the BAC containing *Pnkd*. 62 kb of flanking sequence 5′ of the ATG start site is present in the BAC and is expected to contain all of the cis-acting regulatory elements leading to expression in a pattern faithful to the endogenous alleles. An internal ribosome entry site (IRES) followed by an enhanced red fluorescent protein gene (IRES/DsRed) was introduced into the 3′ UTR of the *Pnkd* gene. The original BAC without mutations was used for generation of *Pnkd* WT-Tg mice. (**B**) Southern blot analyses of mutant and WT-Tg mice. (**C**) Western blot analyses of brain extracts from mut-Tg and WT-Tg mice with C-terminal antibody. Tubulin was used as loading control. (**D**) *Pnkd*-KO mice. A short homologous arm upstream of exon 5 and a long homologous arm downstream of exon 9 were amplified and subcloned into the pMCIDT-A PGKNeo vector to replace 1.5 kb of genomic *Pnkd* DNA (including exons 5–9) with a neomycin resistance gene. (**E**) Genotype analyses of *Pnkd*-KO mice by RT-PCR. (**F**) Western blot analyses of mut-Tg and KO mice using C-terminal antibody. Tubulin was used as loading control. *Pnkd-L (~47 kDa); **Pnkd-M (~40 kDa).

to stress and caffeine was assessed by conventional microdialysis. Consistent with the no net flux method, a significant reduction in extracellular dopamine concentrations in mut-Tg mice was seen both before and after challenge with stress and caffeine (Figure 5C). Two-factor ANOVA with repeated measures revealed a significant effect of genotype ($F_{1,15} = 10.8$; $P < 0.005$), but no effect of treatment ($F_{2,30} = 0.3$; $P < 0.5$). Interestingly, dopamine release in response to stress and caffeine (described as proportion of baseline release) was higher than in WT littermates (Figure 5D). These results indicate that abnormalities in dopamine release at rest and in response to different challenges are present in the striata of Pnkd mice.

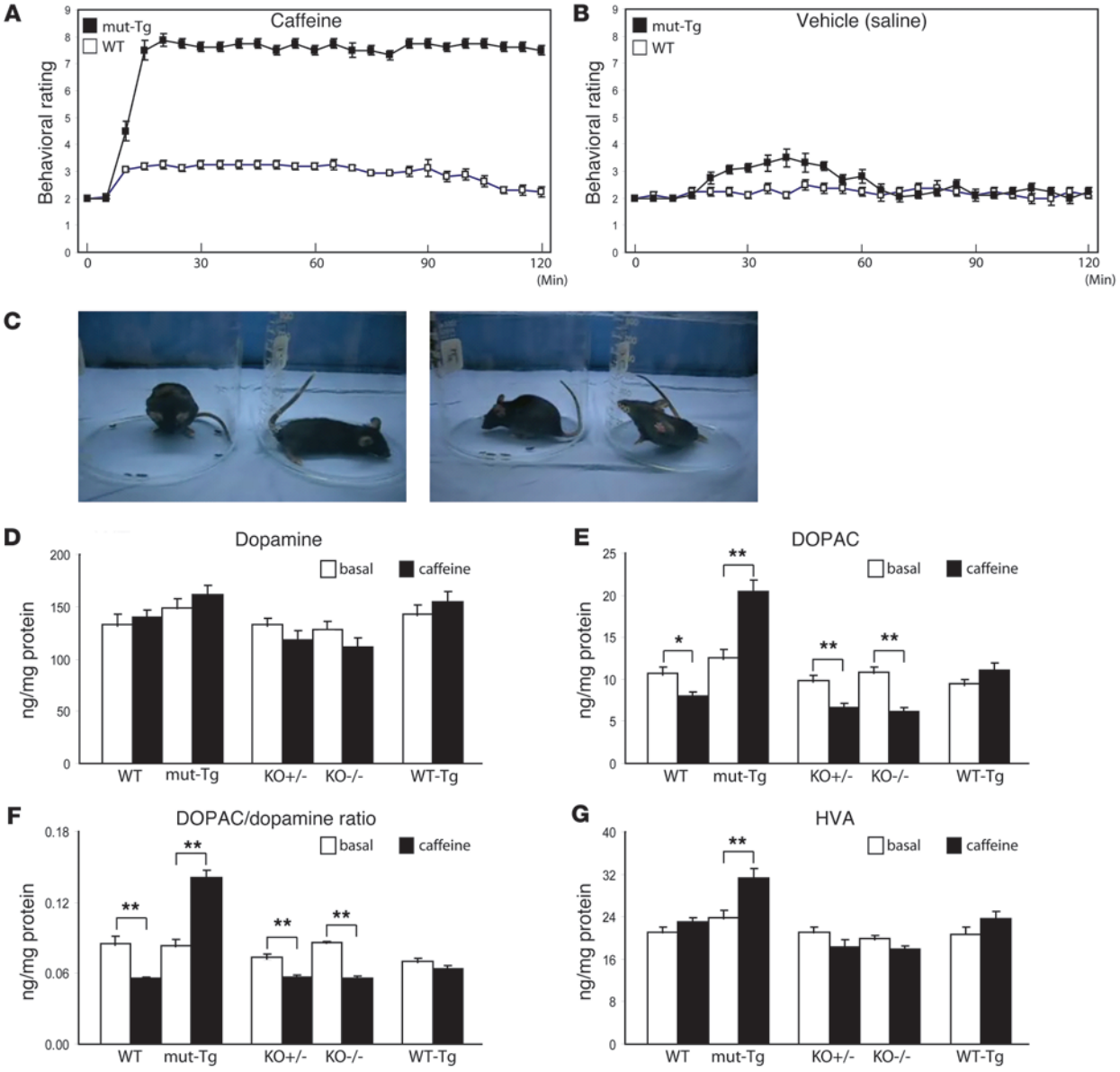

Figure 4

Pnkd mutant mice (mut-Tg, Pnkd mice) recapitulate the PNKD phenotype and have altered dopamine signaling. (**A**) Quantifying activity of Pnkd mice and WT littermates after caffeine injection (25 mg/kg, i.p.). Caffeine-induced hyperkinetic movements in mutant mice. (**B**) Activity ratings of Pnkd mice and WT littermates after saline injection (10 ml/kg, i.p.). A slight increase in activity was observed in Pnkd mice 30–50 minutes after saline injection. (**C**) The mut-Tg mice manifested profound dyskinesia after injection of ethanol (1.5 g/kg, 20% v/v, i.p.), but the same treatment failed to induce hyperkinetic movements in WT littermates. Activity ratings are expressed as mean ± SEM ($n = 8$ for each group). (**D**) There were no obvious differences in the dopamine levels in striatal extracts from mice of various genotypes at rest or after caffeine treatment. (**E** and **F**) Both DOPAC levels and DOPAC/dopamine ratios were significantly increased in Pnkd mice ($P < 0.01$) after caffeine treatment, but decreased in WT and KO mice ($P < 0.01$). (**G**) The HVA levels at rest versus after caffeine treatment were significantly increased in Pnkd mice ($P < 0.05$). All data are presented as mean ± SEM. *$P < 0.05$; **$P < 0.01$.

Pnkd mice have deficits in nigrostriatal neurotransmission. We next performed carbon fiber amperometry studies to assess evoked release of dopamine in striatal slices from mutant and control mice. Electrically evoked release of dopamine was assessed by amperometry in striatal slices. The amperometry traces of striatal slices showed obvious differences between Pnkd mice and WT littermates (Figure 6A). Significantly lower dopamine signals were observed in PNKD mice versus controls ($P < 0.01$; Figure 6B). Application of the selective DAT inhibitor, nomifensine (3 μM/l for 30 minutes), did not significantly increase the dopamine signals in slices from mutant mice compared with slices from WT littermates ($P < 0.01$; Figure 6C). Dopamine release in response to electric stimulation was also significantly lower in slices from Pnkd mice versus WT littermates ($P < 0.05$; Figure 6D). Overall stimulated dopamine

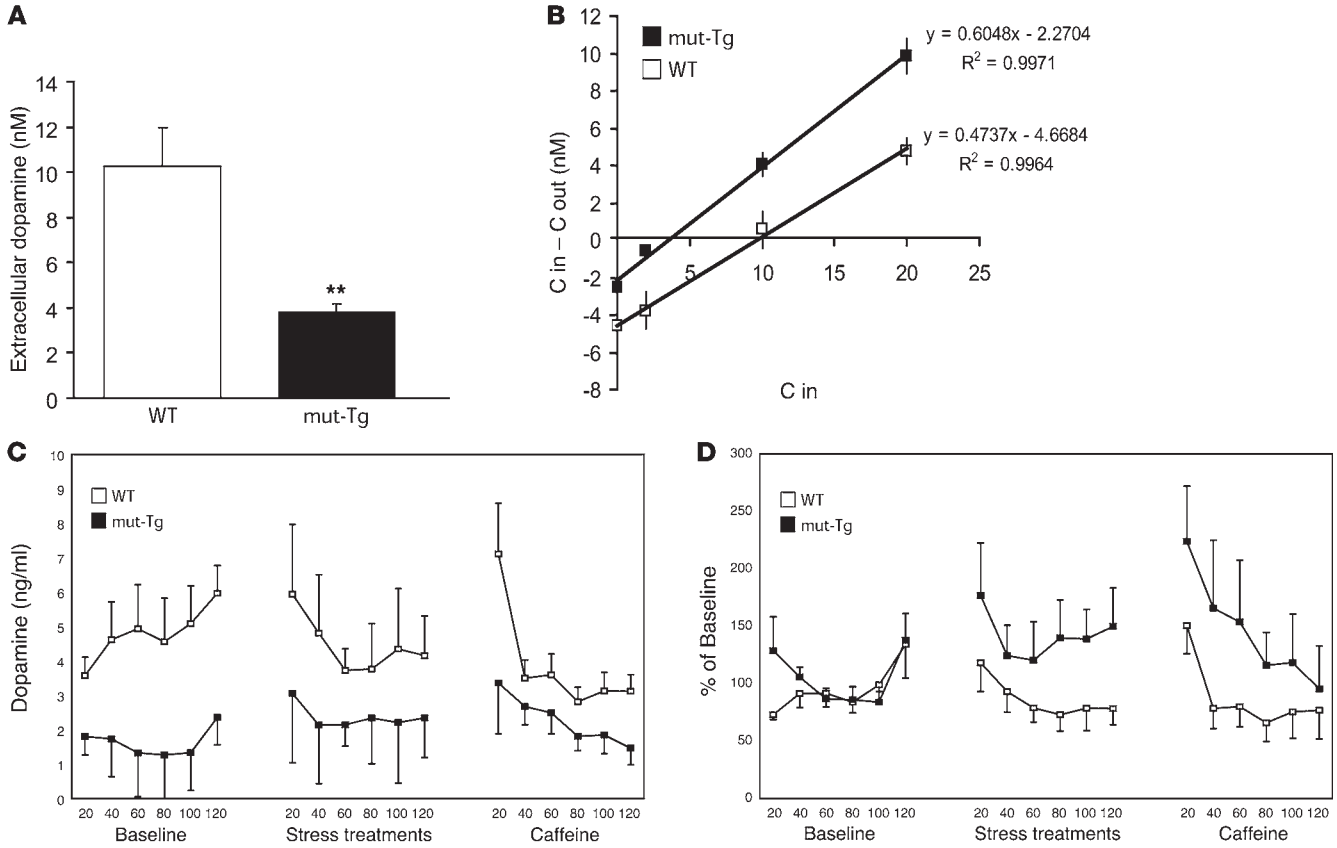

Figure 5

In vivo microdialysis of Pnkd mice. (**A**) Striatal dopamine concentrations were measured by no net flux microdialysis (mut-Tg, $n = 7$; WT, $n = 5$). Decreased levels of extracellular dopamine were observed in striata of Pnkd mice ($P < 0.005$). ** $P < 0.01$. (**B**) No significant difference in extraction fractions was found between genotypes. (**C**) Dopamine concentrations at basal levels and after stress/caffeine stimulation were reduced in striata of Pnkd mice ($P < 0.005$, $n = 7$) versus controls ($n = 5$). (**D**) Higher levels of dopamine release in response to stress and caffeine injection were observed in striata of Pnkd versus WT mice ($P < 0.05$). All data are shown as mean ± SEM.

release was restored to normal levels in Pnkd slices after application of nomifensine. The spike width was significantly smaller and the half width ($t_{1/2}$) was significantly larger in Pnkd than in WT controls ($P < 0.05$; Figure 6, D and E). The spike width returned to normal in the presence of nomifensine (Figure 6D), but the $t_{1/2}$ did not ($P < 0.01$; Figure 6E). These results suggest that Pnkd mice feature significant deficits in nigrostriatal neurotransmission characterized by low levels of dopamine release and enhanced dopamine reuptake. The latter is compatible with DAT expression being significantly higher in the Pnkd mice compared with WT littermates (Supplemental Figure 4E).

Neuropharmacologic characterization of Pnkd mice. Striatal A_1R and $A_{2A}R$ are the major modulators of striatal signaling (20, 21). The A_1Rs are enriched in striatonigral-striatoentopenduncular medium spiny neurons that constitute the direct output pathway expressing dopamine D_1 receptors (D_1Rs). $A_{2A}Rs$ and dopamine D_2 receptors (D_2Rs) are both expressed in striatopallidal medium spiny neurons that represent the indirect output pathway (22–24). Since caffeine is a nonselective adenosine receptor antagonist (25–27), we evaluated the contribution of A_1R and $A_{2A}R$ to attacks in PNKD. Dyskinesias were induced in Pnkd mice approximately 20 minutes after i.p. injection of the selective $A_{2A}R$ antagonist 8-(3-chlorostryl) caffeine (CSC) (5 mg/kg; Figure 7A) and lasted approximately 2 hours. The A_1R antagonist 8-cyclopentyl-1,3-dipropylxanthine (DPCPX) (3 mg/kg) did not induce dyskinesias in Pnkd mice (Figure 7B). The A_1R agonist N6-cyclopentyladenosine (CPA) (0.1 mg/kg) had no obvious effects on Pnkd mice or controls (Supplemental Figure 6A), and the $A_{2A}R$ agonist 2p-(2 carboxyethyl)phenethylamine-5′-N-ethylcarboxyamindoadenosine (CGS 21680) (0.5 mg/kg) led to a reduction of activity in both Pnkd mice and controls, with no difference between genotypes (Supplemental Figure 6B).

We speculated that dyskinesias induced by caffeine are caused by altered signaling between adenosine receptors and dopamine receptors in striatum. D_1R and D_2R are major receptors in the regulation of striatal function, and antagonistic interactions between A_1R-D_1R and $A_{2A}R$-D_2R in the basal ganglia are important in motor control (13). Since D_2Rs colocalize with $A_{2A}Rs$ in neurons of the indirect pathway of the striatum, we hypothesized that the selective D_2R agonist quinpirole would induce dyskinetic attacks in Pnkd mice. Mutant mice developed dyskinesias approximately 15 minutes after quinpirole treatment (2.5 mg/kg), but no phenotype was seen in controls (Figure 7C). The D_1R agonist SKF 82958 (0.75 mg/kg) increased the behavioral activity in all mice, without significant differences among genotypes (Figure 7D). Taken together, these results support a model of adenosine-dopamine signaling dysregulation in PNKD.

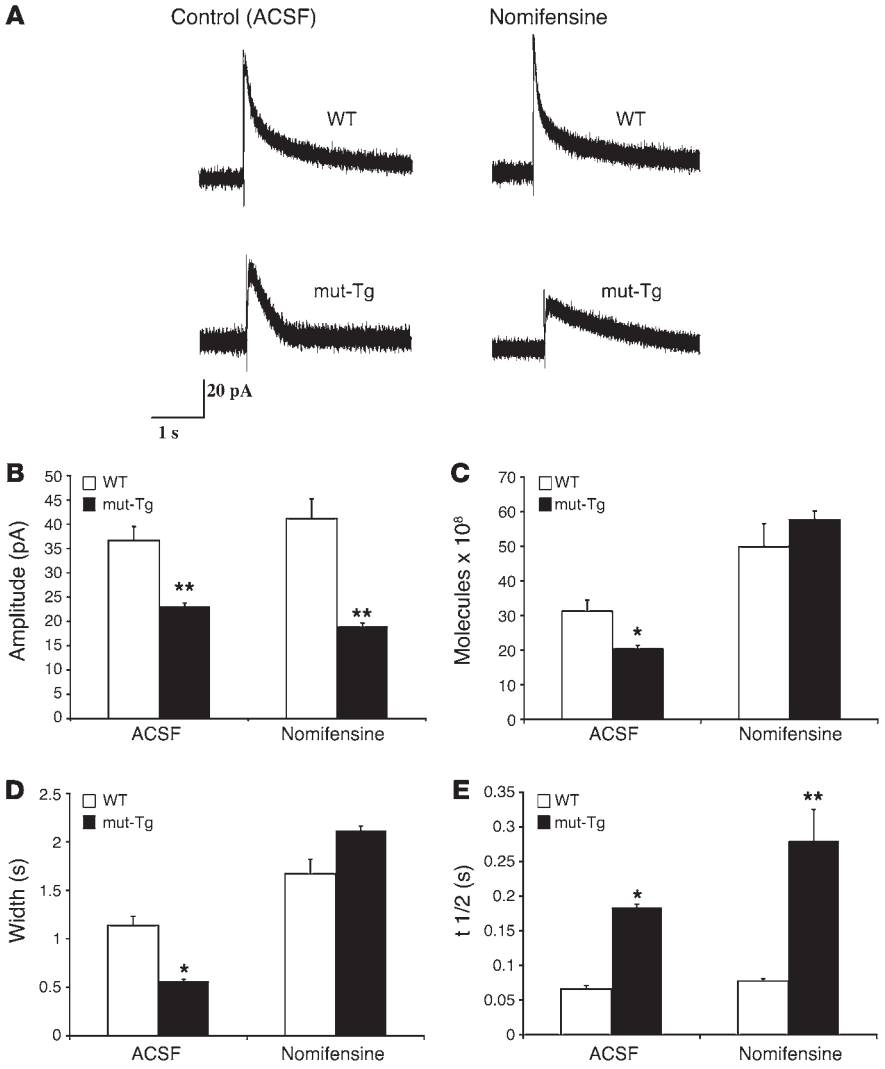

Figure 6
Amperometry studies of Pnkd mice. (**A**) The amperometry traces of Pnkd mice versus WT littermates. (**B**) The mean evoked dopamine signal amplitude was significantly decreased in striatal slices from Pnkd mice versus controls with or without nomifensine ($P < 0.01$). (**C**) Striatal slices from Pnkd mice showed significantly reduced dopamine release per stimulation ($P < 0.05$). Application of nomifensine restored the overall stimulated dopamine release. (**D** and **E**) Striatal slices of Pnkd mice showed significant reduction of the spike width and elevated half width ($t_{1/2}$) of dopamine release ($P < 0.05$). Only the spike width of Pnkd slices was restored in the presence of nomifensine. In contrast, application of nomifensine did not restore the half width of Pnkd mouse striatal slices ($P < 0.01$). All data are presented as mean ± SEM. * $P < 0.05$; ** $P < 0.01$.

Discussion

PNKD is a rare disorder in which dyskinetic attacks can be induced by ingestion of caffeine or alcohol and frequently when patients are stressed (3). A transgenic Pnkd mouse model carrying both human mutations recapitulates the human phenotype. *Pnkd*-KO mice do not have a phenotype, arguing that the mutation of PNKD is a gain-of-function allele. It is possible that these *PNKD* mutations cause the disease by altering enzyme activity or specificity. Alternatively, they may not alter its enzymatic properties, but rather, cause altered trafficking and localization of the protein in neurons or through alterations of interactions between PNKD-L and other neuronal proteins. Finally, it is also possible that PNKD has evolved a novel function and is not an enzyme.

We presented in vivo evidence of increased dopamine turnover. Administration of caffeine has been shown to increase dopamine release accompanied by decreased DOPAC levels in rat striatum (28–30), similar to what we saw in WT control and *Pnkd*-KO mice. It is also known that acute ethanol administration can cause an increase of dopamine turnover as assessed by increased DOPAC in rat striatum, suggesting that both pre- and postsynaptic dopaminergic mechanisms may be involved in the mediation of some of the central effects of ethanol in striatum (31, 32). Increased c-Fos expression in basal ganglia of mutant versus control mice after caffeine administration shows that neurons in this part of brain are activated with the induction of attacks. Furthermore, Pnkd mice have significantly lower evoked dopamine release in real time and higher expression levels of dopamine receptors, DAT, and MAO-B in the striatum compared with controls. Taken together, these results suggest dysfunction of dopamine signaling in basal ganglia of Pnkd mice with induction of dyskinesias.

Neuropharmacological experiments implicate a role for A_{2A}Rs and D_2Rs in pathogenesis, as attacks can be triggered with a selective A_{2A}R antagonist and a selective D_2R agonist. This, in turn, leads to dysfunction of antagonistic interactions between adenosine and dopamine receptors in modulation of motor outputs from striatum (22, 24). These results indicate strong involvement of the striatal indirect pathway in PNKD pathophysiology, but we cannot rule out the possibility that the direct pathway is also involved. Furthermore, though it is clear that the striatum is important for transducing abnormal dopamine signaling in PNKD, both A_{2A} and D_2 receptors are also expressed in other CNS regions. Besides, adenosine A1Rs are expressed presynaptically in CNS, including

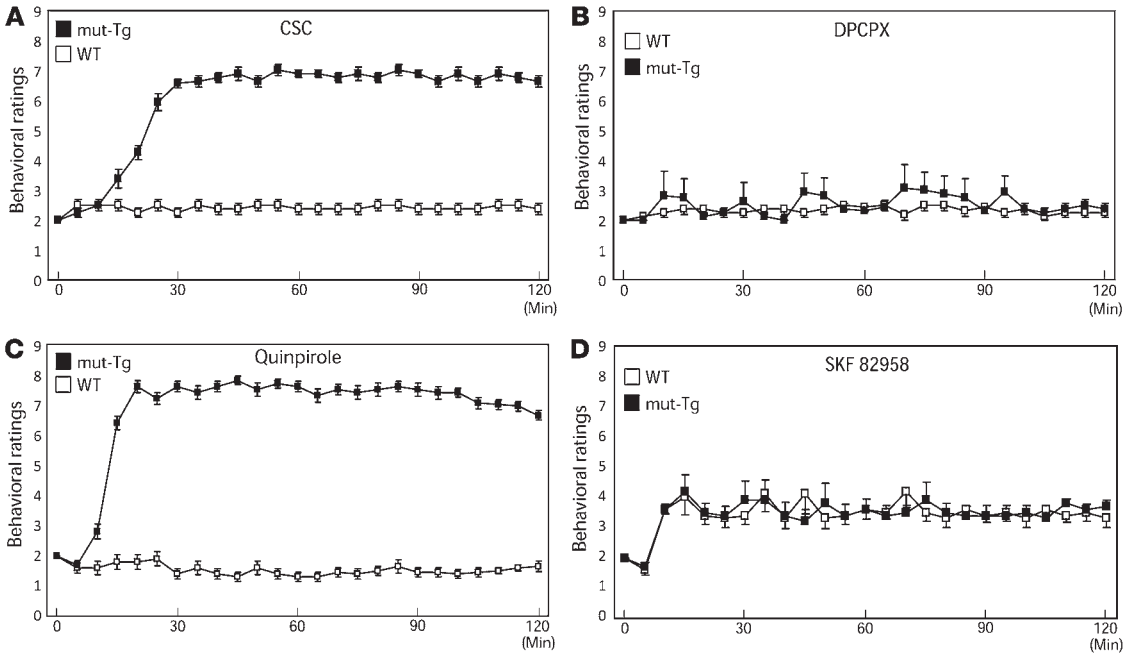

Figure 7
Pharmacological studies of Pnkd mice. (**A**) There are significant hyperkinetic movements in Pnkd (mut-Tg) mice (versus littermate controls) after injection of the adenosine A_2 receptor antagonist CSC (5 mg/kg, i.p.). (**B**) No difference in activity ratings of Pnkd mice and WT littermates was observed after injection of the adenosine A_1 receptor antagonist DPCPX (3 mg/kg, i.p.). (**C**) There are significant hyperkinetic movements in Pnkd mice after injection of the dopamine D_2 receptor agonist quinpirole (2.5 mg/kg, i.p.). (**D**) Increased activity was observed in both Pnkd mice and WT controls after injection of SKF 82958 (D_1 receptor agonist, 0.75 mg/kg, i.p.), but no difference was found between genotypes. In all pharmacological studies, behavioral ratings are expressed as mean ± SEM (n = 8 for each group).

at glutamatergic terminals on medium spiny neurons. Thus, the genesis of PNKD could be outside the striatum (e.g., cortex).

Alterations of dopaminergic function in striatum play an important role in primary dystonias. Dopa-responsive dystonia (DYT5) is caused by mutations of the *GTP–cyclohydrolase 1* gene involved in catecholamine and serotonin biosynthesis or by mutations of *TH* (2, 33). In dt^{sz} hamsters, an elevation of extracellular striatal dopamine levels has been observed during dystonic episodes (34). Interestingly, unlike dt^{sz} hamsters, Pnkd mice have reduced extracellular dopamine in striatum in vivo, but, when challenged by stress, caffeine, or alcohol, there is a relative increase in dopamine compared with controls. Pnkd mice have normal dopamine content in striatal dopaminergic terminals and apparently normal dopamine production. But dopamine receptors are upregulated, and when animals are stressed, striatal dopamine release is increased in Pnkd mice and receptor sensitivity is increased due to low basal extracellular dopamine levels. Excessive dopaminergic signaling under these conditions may lead to abnormal neuronal activity in Pnkd basal ganglia accompanied by significantly increased dopamine turnover. Although, typically, less dopamine release might be expected to yield less movement, dopamine loss occurring early in development can result in abnormal and excessive movements. This is true in humans with DYT5, where a developmental loss of dopamine caused by mutations that reduce dopamine synthesis causes dystonia (35, 36). It is also true for rodents, since dopamine depletion by 6-hydroxydopamine (6-OHDA) in adult rats causes akinesia (37–39). However, neonatal 6-OHDA treatment in rats causes hyperactivity (40–42).

PNKD-L is a membrane-associated protein, and Pnkd mice exhibit alterations of exocytosis, suggesting that PNKD may be involved in modulation of neurotransmitter release at nigrostriatal dopaminergic terminals. Alternatively, PNKD may participate in the modulation of striatal glutamatergic inputs projecting from cerebral cortex and thalamus. Adenosine receptors and dopamine receptors not only interact with each other, but also cooperate with other signaling systems, such as metabotropic glutamate receptors and cannabinoid receptors. These interactions between different signaling systems are critical for modulation of normal striatal function and plasticity (14, 20, 43, 44). These findings imply that dysfunction of the striatal dopamine signaling system plays a pivotal role in PNKD pathophysiology. Although expression levels of adenosine receptors and glutamate transporters are not different in striatum of Pnkd mice, we cannot rule out the possibility of altered sensitivity of adenosine receptors and/or glutamate release in glutamatergic terminals. Dopamine is critical for the induction of bidirectional plasticity at glutamatergic synapses on the medium spiny neurons of both direct and indirect pathways, and this balance is interrupted in models of Parkinson disease that cause unidirectional changes in striatal synaptic plasticity (45). Glutamatergic synapses onto the medium spiny neurons of the indirect pathway show higher release probability than glutamatergic synapses onto the medium spiny neurons of the direct pathway, and they selectively express endocannabinoid-mediated long-term depression that is absent in a model of Parkinson disease (46). Since the striatal dopamine signaling system may be upregulated, Pnkd mice may also display alterations of

striatal synaptic plasticity under stress or with caffeine/ethanol treatment. In turn, transient alterations of neuronal activity in basal ganglia may occur during PNKD attacks. Further study will provide better understanding of the role of the PNKD protein in cellular and synaptic regulation and contribution of PNKD mutations to pathophysiology. Such work may allow development of better therapies for PNKD and potentially for other episodic disorders. Since *PNKD* is a novel gene participating in modulating striatal neurotransmitter release, further investigations both in vitro and in vivo will give new insights into understanding normal basal ganglia regulation of motor function and potentially have implications for developing an understanding other dystonias and striatal diseases.

Methods

Study approval. All animal studies were approved by the Animal Care and Use Committee at UCSF.

PNKD antibodies. Polyclonal antibodies were developed (Covance) using 2 synthesized oligopeptides corresponding to the N terminus of PNKD-L and -S and the C terminus of PNKD-L and -M. Preimmune bleeds and test bleeds were obtained individually from the supplier to monitor antibody titer and specificity in subsequent bleeds. Antibodies were affinity purified using standard procedures (see Supplemental Methods). Affinity-purified antibodies were then used for Western blotting and immunohistochemistry experiments (N-terminal antibody, 1:250 to 1:500 dilution; C-terminal antibody, 1:500 to 1:1000 dilution).

Generation of Pnkd-transgenic and -KO mice. Both mut-Tg and WT-Tg (as a dosage control) mice were generated (details in Supplemental Methods). The transgene copy number was estimated by Southern blotting. Tail DNA or control DNA spiked with BAC DNA representing 1, 3, 5, 10, and 30 copies/genome was digested with *Pst*I, electrophoresed on 0.8% agarose, and transferred to a Hybond-N+ membrane. Blots were hybridized with a random primed ^{32}P-dCTP-labeled probe amplified from the BAC clone. Primers and conditions for RT-PCR are detailed in the Supplemental Methods.

Immunohistochemistry in mouse brain and transfected cells. WT and transgenic male mice were sacrificed and perfused; brains/spinal cords were removed, fixed, postfixed, and cryoprotected, and 14-μm coronal sections were cut and mounted using standard techniques. Blots were probed with anti-PNKD C- or N-terminal antibody and colabeled with mouse monoclonal antibodies for detection of either neuron-specific nuclear protein (NeuN), glial fibrillary acidic protein (GFAP), myelin basic protein (MBP), dopamine- and cAMP-regulated neuronal phosphoprotein with molecular weight 32 kDa (DARPP-32), choline acetyltransferase (ChAT), parvalbumin, glutamic acid decarboxylase isoform 67 (GAD67), or TH (see Supplemental Methods). After washing, sections were then incubated with fluorescent secondary antibodies, washed, and mounted; images were captured with a Zeiss Pascal LSM5 confocal microscope in the UCSF microscopy core. Images were analyzed in Photoshop (Adobe Systems). Human embryonic kidney 293 (HEK293) cells were transfected with 2 μg DNA (*PNKD*-L fusion constructs), grown, fixed, and probed with appropriate antibodies using a standard protocol (see Supplemental Methods). Images were acquired using the Zeiss Pascal LSM5 confocal microscope in the UCSF microscopy core facility.

Immunoblotting of transfected cells. HEK293 cells were transfected with 2 μg DNA (*PNKD-L*, *-M*, and *-S* WT fusion constructs), grown, and harvested 36 hours later, after transfection. HEK cells were sonicated in 500 μl of RIPA buffer with protease and phosphatase inhibitors; then the homogenates were used for Western blots incubated with PNKD antibodies and rabbit anti-GFP antibody (1:5000 dilution; Abcam). For the detergent phase partitioning experiments, the crude membrane fractions of transfected HEK293 cells were collected. TX-114 was added into crude membrane fractions and incubated; 2 layers (hydrophobic and hydrophilic) were collected as described (47, 48) and then were used in Western blots.

Immunoblotting of mice brain tissues. Western blotting of whole-brain tissue homogenates obtained from WT, transgenic, and KO mice was performed using standard techniques detailed in the Supplemental Methods. Pnkd levels were normalized to α-tubulin using the average pixel intensity for immunoreactive bands in each lane, and the images were analyzed by NIH ImageJ software. Dorsal striata of mice (n = 8/genotype) were dissected and snap-frozen in liquid nitrogen, then sonicated in 300 μl of buffer with protease and phosphatase inhibitors. Blots were then incubated with antibodies raised against the following proteins: VGLUT1, Rab3A, synaptophysin, EAAT3, MAO-A, MAO-B, ADK, adenosine A_1 receptor, COMT, synapsin-1, GAD65, GAD67, adenosine A_{2A} receptor, TH, DAT, dopamine D_{1A} and D_2 receptors, and VMAT2 (details in Supplemental Methods). After detection, blots were stripped and reprobed with either anti–α-tubulin or anti–glyceraldehyde 3-phosphate dehydrogenase antibodies. Striata protein levels were normalized, and data were analyzed using Student's t test.

Mapping of c-Fos induction after precipitation of a PNKD attack. Based on pilot tests for time course, a 2-hour time point was selected to examine c-Fos immunoreactivity after i.p. injection of ethanol or caffeine. Mice were perfused intracardially under deep 2,2,2-tribromoethanol (Avertin) alcohol anesthesia using standard protocols. Brain slices were incubated with anti-cFos primary and appropriate secondary antibodies (see Supplemental Methods). Images were captured with a Nikon Eclipse microscope and CCD camera or a Leica DM5000B microscope with a SPOT RT camera (SPOT diagnostic Inc.) and imported into Photoshop for analysis. Neuroanatomical studies were conducted in a blinded manner.

Detection of biogenic amines in striatum by HPLC. Pnkd mice, WT littermates, *Pnkd* WT-Tg mice, and *Pnkd*-KO mice were sacrificed under basal conditions (10–12 mice per genotype) or 20 minutes after i.p. injection of caffeine (25 mg/kg; 10–12 mice for each genotype). Striata were quickly removed, frozen in liquid nitrogen, and stored at –80°C prior to HPLC. Dorsal striata were homogenized in 100–750 μl of 0.1M TCA containing 10^{-2} M sodium acetate, 10^{-4} M EDTA, and 10.5% methanol (pH 3.8). Samples were spun in a microcentrifuge at 10,000 g for 20 minutes. The supernatant was removed and stored at –80°C, and the pellet was saved for protein analysis. Supernatant was then thawed and spun for 20 minutes, and supernatant samples were analyzed for biogenic monoamines and/or amino acids using a specific HPLC assay with an Antec Decade II (oxidation: 0.5) electrochemical detector operated at 33°C. Then 20-μl samples of the supernatant were injected using a Water 717+ autosampler onto a Phenomenex Nucleosil (5 μl, 100A) C18 HPLC column (150 × 4.60 mm). Biogenic amines were eluted with a mobile phase consisting of 89.5% 0.1 M TCA, 10^{-2} M sodium acetate, 10^{-4} M EDTA and 10.5 % methanol (pH 3.8). Solvent was delivered at 0.6 ml/min using a Waters 515 HPLC pump. HPLC control and data acquisition were managed by Millennium 32 software. Two-way ANOVA was used for analyzing the results.

In vivo microdialysis. Microdialysis was performed in alert, freely moving mice. After anesthesia with tribromoethanol and positioning in a stereotaxic frame (Stoelting), a microdialysis probe was implanted in the striatum (+0.6 AP, +1.7 ML, 4.5 DV) as previously described (49). After surgery, the probe was perfused continuously with artificial cerebrospinal fluid (ACSF: 147 mM NaCl, 3.5 mM KCl, 1.2 mM $CaCl_2$, 1.2 mM $MgCl_2$, 1 mM NaH_2PO_4, and 25 mM $NaHCO_3$, pH 7.0-7.4) at a flow rate of 0.6 μl/minute. For conventional microdialysis, samples were collected 12–15 hours after surgery at 20-minute intervals, and 6 consecutive samples were collected as baseline. To determine the effect of stress on dopamine overflow, mice were then injected with saline (10 ml/kg, i.p.) and transferred to a novel cage. Six samples were collected after injection at 20-minute intervals. Then, 2 hours after

stress challenge, mice were injected with 25 mg/kg caffeine (10 ml/kg, s.c.) and 6 samples were collected at 20-minute intervals. For no net flux microdialysis, after implantation, the probe was perfused with ACSF plus 250 μM ascorbic acid at a flow rate of 0.6 μl/min overnight. On the day of the experiment, the probe was perfused at the same rate with perfusate plus different concentrations of dopamine (0, 2, 10, or 20 nM; C_{in}) in pseudo-random order. After a 25-minute equilibration period, 3 samples were collected (C_{out}). The dopamine concentration in the perfusate was then switched and the process repeated until all dopamine concentrations were tested. The location of the probe within the striatum was confirmed histologically.

Samples were analyzed by HPLC (MD-150 column, 150 mm length; 3 mm I.D.; ESA) with a 5014B microdialysis cell. The mobile phase was composed of 1.7 mM 1-octanesulfonic acid sodium salt, 25 μM EDTA, 75 mM NaH_2PO_4, and 8% acetonitrile (pH 2.9) with a flow rate of 0.6 ml/min. Neurotransmitters and metabolites were identified by matching retention time to that of known standards. For no net flux microdialysis, data were subjected to a linear regression analysis of $C_{in} - C_{out}$ versus C_{in}. The x-intercept provides an unbiased estimate of extracellular dopamine concentration. Data were analyzed using 2-factor ANOVA or Student's *t* test, where appropriate.

Amperometry studies of Pnkd mice. Brain slice recordings were performed using standard protocols detailed in the Supplemental Methods. Details of the brain slice amperometric recordings have been described (50, 51). Local bath application of the dopamine reuptake blocker nomifensine (3 μM) for at least 30 minutes was used to access the contribution of reuptake in the evoked dopamine signal. Five signal pulses/slice were averaged into a grand mean, and the 2 groups (Pnkd mice vs. WT littermates) were compared with 1-way ANOVA of the mean.

Pharmacology studies. To evaluate the response of mice to caffeine and ethanol, the triple stimulation technique was modified from Richter and Loscher (52). This procedure consists of (a) removing mice from home cages and placing them on a balance; (b) i.p. injection of saline or other drugs; and (c) placement of the animals into an empty 1000-ml glass beaker or empty cage (1 animal per beaker/cage). Mice were observed for 2 hours after stimulation. Drug effects were examined in Pnkd mice and WT littermates (8 mice/genotype). Each group was used for 1 to 2 doses (with more than 1 week between doses). A control trial was undertaken with the triple stimulation technique, injecting the vehicle used for i.p. drug administration (predrug control). Two days later, the drug was administered in the same group of animals. As described for predrug controls, a control trial with vehicle was done 2 days after treatment (postdrug control). All trials were done between 1300 and 1700 hours. Test reagents were administered i.p. Ethanol was diluted and injected at 1.5 g/kg (20% w/v in 0.9% saline). The nonselective adenosine receptor antagonist caffeine (25 mg/kg), the D_1 dopamine receptor agonist Chloro-APB hydrobromide (SKF 82958, 0.75 mg/kg), and the D_2 dopamine receptor agonist quinpirole (2.5 mg/kg) were dissolved in 0.9% saline. The adenosine A_1 receptor antagonist DPCPX (3 mg/kg), the A_{2A} antagonist CSC (5 mg/kg), the adenosine A_1 receptor agonist CPA (0.1 mg/kg), and the A_{2A} receptor agonist CGS 21680 (0.5 mg/kg) were dissolved in 10% DMSO/10% Cremophor El (Fisher Scientific). All solutions and suspensions were freshly prepared, and injection volumes were 10 ml/kg (10 μl/g body weight). The severity of the phenotype was rated by the following scoring system modified from Wang and McGinty (53): (a) asleep, inactive; (b) normal activity, grooming; (c) increased activity; (d) hyperactivity, running; (e) jerky movement and slow patterned movement (repetitive exploration); (f) fast patterned movement (repetitive exploration with hyperactivity); (g) stereotyped movements (repetitive sniffing/rearing in one location); (h) continuous gnawing, sniffing and/or licking; and (i) dyskinesia, seizures. The behavior of the mice was rated before the drug injection and every 5 minutes during the entire test period. Predrug and postdrug control trials were undertaken in the same animals 2 days before and 2 days after drug testing. All neuropharmacological testing was done in a blinded manner.

Statistics. All values are shown as mean ± SEM, and data were statistically analyzed by 1-way ANOVA (amperometry studies and pharmacology studies), 2-way ANOVA (studies of biogenic amines in striatum and in vivo microdialysis), or 2-tailed Student's *t* test (Western blot analysis and in vivo microdialysis). *P* values of 0.05 or less were considered statistically significant.

Acknowledgments

We thank Anatol Kreitzer and Shu-Ting Lin for helpful discussions. This work was supported by grants from the Dystonia Medical Research Foundation, the Bachmann-Strauss Dystonia & Parkinson Foundation, NIH grant U54 RR19481, the Sandler Neurogenetics Fund, and P30 NS047243 (Tufts Center for Neuroscience Research). L.J. Ptácek is an investigator of the Howard Hughes Medical Institute.

Received for publication April 13, 2011, and accepted in revised form November 16, 2011.

Address correspondence to: Louis Ptácek or Ying-Hui Fu, Department of Neurology, UCSF MC 2922, 548F Rock Hall, 1550 Fourth St., San Francisco, California 94158-2324, USA. Phone: 415.502.5614; Fax: 415.502.5641; E-mail: ljp@ucsf.edu (L. Ptácek); ying-hui.fu@ucsf.edu (Y.-H. Fu).

Junko Nakayama's present address is: Department of Pediatrics, Ibaraki Prefectural University of Health Sciences, Ibaraki, Japan.

Ying Xu's present address is: Model Animal Resource Center, Nanjing University, Nanjing, China.

1. Demirkiran M, Jankovic J. Paroxysmal dyskinesias: clinical features and classification. *Ann Neurol*. 1995;38(4):571–579.
2. Tarsy D, Simon DK. Dystonia. *N Engl J Med*. 2006;355(8):818–829.
3. Bruno MK, et al. Genotype-phenotype correlation of paroxysmal nonkinesigenic dyskinesia. *Neurology*. 2007;68(21):1782–1789.
4. Fink JK, et al. Paroxysmal dystonic choreoathetosis: tight linkage to chromosome 2q. *Am J Hum Genet*. 1996;59(1):140–145.
5. Fouad GT, Servidei S, Durcan S, Bertini E, Ptacek LJ. A gene for familial paroxysmal dyskinesia (FPD1) maps to chromosome 2q. *Am J Hum Genet*. 1996;59(1):135–139.
6. Chen DH, et al. Presence of alanine-to-valine substitutions in myofibrillogenesis regulator 1 in paroxysmal nonkinesigenic dyskinesia: confirmation in 2 kindreds. *Arch Neurol*. 2005;62(4):597–600.
7. Lee HY, et al. The gene for paroxysmal non-kinesigenic dyskinesia encodes an enzyme in a stress response pathway. *Hum Mol Genet*. 2004;13(24):3161–3170.
8. Stefanova E, et al. Clinical characteristics of paroxysmal nonkinesigenic dyskinesia in Serbian family with Myofibrillogenesis regulator 1 gene mutation. *Mov Disord*. 2006;21(11):2010–2015.
9. Rainier S, et al. Myofibrillogenesis regulator 1 gene mutations cause paroxysmal dystonic choreoathetosis. *Arch Neurol*. 2004;61(7):1025–1029.
10. Hempelmann A, Kumar S, Muralitharan S, Sander T. Myofibrillogenesis regulator 1 gene (MR-1) mutation in an Omani family with paroxysmal nonkinesigenic dyskinesia. *Neurosci Lett*. 2006;402(1–2):118–120.
11. Ghezzi D, et al. Paroxysmal non-kinesigenic dyskinesia is caused by mutations of the MR-1 mitochondrial targeting sequence. *Hum Mol Genet*. 2009;18(6):1058–1064.
12. Thornalley PJ. Pharmacology of methylglyoxal: formation, modification of proteins and nucleic acids, and enzymatic detoxification--a role in pathogenesis and antiproliferative chemotherapy. *Gen Pharmacol*. 1996;27(4):565–573.
13. Fisone G, Hakansson K, Borgkvist A, Santini E. Signaling in the basal ganglia: postsynaptic and presynaptic mechanisms. *Physiol Behav*. 2007;92(1–2):8–14.
14. Surmeier DJ, Ding J, Day M, Wang Z, Shen W. D1 and D2 dopamine-receptor modulation of striatal glutamatergic signaling in striatal medium spiny neurons. *Trends Neurosci*. 2007;30(5):228–235.
15. Werkman TR, Glennon JC, Wadman WJ, McCreary AC. Dopamine receptor pharmacology: interactions with serotonin receptors and significance for the aetiology and treatment of schizophrenia. *CNS Neurol Disord Drug Targets*. 2006;5(1):3–23.

16. Bolam JP, Hanley JJ, Booth PA, Bevan MD. Synaptic organisation of the basal ganglia. *J Anat*. 2000;196(pt 4):527–542.
17. Mink JW. The basal ganglia: focused selection and inhibition of competing motor programs. *Prog Neurobiol*. 1996;50(4):381–425.
18. Smith Y, Bevan MD, Shink E, Bolam JP. Microcircuitry of the direct and indirect pathways of the basal ganglia. *Neuroscience*. 1998;86(2):353–387.
19. Lundstrom K, Salminen M, Jalanko A, Savolainen R, Ulmanen I. Cloning and characterization of human placental catechol-O-methyltransferase cDNA. *DNA Cell Biol*. 1991;10(3):181–189.
20. Schiffmann SN, Fisone G, Moresco R, Cunha RA, Ferre S. Adenosine A2A receptors and basal ganglia physiology. *Prog Neurobiol*. 2007;83(5):277–292.
21. Schwarzschild MA, Agnati L, Fuxe K, Chen JF, Morelli M. Targeting adenosine A2A receptors in Parkinson's disease. *Trends Neurosci*. 2006; 29(11):647–654.
22. Fuxe K, Ferre S, Genedani S, Franco R, Agnati LF. Adenosine receptor-dopamine receptor interactions in the basal ganglia and their relevance for brain function. *Physiol Behav*. 2007;92(1–2):210–217.
23. Ferre S, Fredholm BB, Morelli M, Popoli P, Fuxe K. Adenosine-dopamine receptor-receptor interactions as an integrative mechanism in the basal ganglia. *Trends Neurosci*. 1997;20(10):482–487.
24. Kim DS, Palmiter RD. Interaction of dopamine and adenosine receptor function in behavior: studies with dopamine-deficient mice. *Front Biosci*. 2008;13:2311–2318.
25. Fisone G, Borgkvist A, Usiello A. Caffeine as a psychomotor stimulant: mechanism of action. *Cell Mol Life Sci*. 2004;61(7–8):857–872.
26. Ferre S. An update on the mechanisms of the psychostimulant effects of caffeine. *J Neurochem*. 2008;105(4):1067–1079.
27. Xie X, Ramkumar V, Toth LA. Adenosine and dopamine receptor interactions in striatum and caffeine-induced behavioral activation. *Comp Med*. 2007;57(6):538–545.
28. Watanabe H, Uramoto H. Caffeine mimics dopamine receptor agonists without stimulation of dopamine receptors. *Neuropharmacology*. 1986; 25(6):577–581.
29. Morgan ME, Vestal RE. Methylxanthine effects on caudate dopamine release as measured by in vivo electrochemistry. *Life Sci*. 1989;45(21):2025–2039.
30. Kirch DG, Taylor TR, Gerhardt GA, Benowitz NL, Stephen C, Wyatt RJ. Effect of chronic caffeine administration on monoamine and monoamine metabolite concentrations in rat brain. *Neuropharmacology*. 1990;29(6):599–602.
31. Reggiani A, Barbaccia ML, Spano PF, Trabucchi M. Dopamine metabolism and receptor function after acute and chronic ethanol. *J Neurochem*. 1980;35(1):34–37.
32. Barbaccia ML, Bosio A, Spano PF, Trabucchi M. Ethanol metabolism and striatal dopamine turnover. *J Neural Transm*. 1982;53(2–3):169–177.
33. Breakefield XO, Blood AJ, Li Y, Hallett M, Hanson PI, Standaert DG. The pathophysiological basis of dystonias. *Nat Rev Neurosci*. 2008;9(3):222–234.
34. Hamann M, Richter A. Striatal increase of extracellular dopamine levels during dystonic episodes in a genetic model of paroxysmal dyskinesia. *Neurobiol Dis*. 2004;16(1):78–84.
35. Clot F, et al. Exhaustive analysis of BH4 and dopamine biosynthesis genes in patients with Dopa-responsive dystonia. *Brain*. 2009;132(pt 7):1753–1763.
36. Segawa M. Dopa-responsive dystonia. *Handb Clin Neurol*. 2011;100:539–557.
37. Marin C, Aguilar E, Mengod G, Cortes R, Obeso JA. Concomitant short- and long-duration response to levodopa in the 6-OHDA-lesioned rat: a behavioural and molecular study. *Eur J Neurosci*. 2007; 25(1):259–269.
38. Paille V, Henry V, Lescaudron L, Brachet P, Damier P. Rat model of Parkinson's disease with bilateral motor abnormalities, reversible with levodopa, and dyskinesias. *Mov Disord*. 2007;22(4):533–539.
39. Zigmond MJ, Berger TW, Grace AA, Stricker EM. Compensatory responses to nigrostriatal bundle injury. Studies with 6-hydroxydopamine in an animal model of parkinsonism. *Mol Chem Neuropathol*. 1989;10(3):185–200.
40. Breese GR, Knapp DJ, Criswell HE, Moy SS, Papadeas ST, Blake BL. The neonate-6-hydroxydopamine-lesioned rat: a model for clinical neuroscience and neurobiological principles. *Brain Res Brain Res Rev*. 2005;48(1):57–73.
41. Fan X, Bruno KJ, Hess EJ. Rodent models of ADHD [published online ahead of print March 15, 2011]. *Curr Top Behav Neurosci*. doi:10.1007/7854_2011_121.
42. Masuo Y, Morita M, Oka S, Ishido M. Motor hyperactivity caused by a deficit in dopaminergic neurons and the effects of endocrine disruptors: a study inspired by the physiological roles of PACAP in the brain. *Regul Pept*. 2004;123(1–3):225–234.
43. Kreitzer AC, Malenka RC. Striatal plasticity and basal ganglia circuit function. *Neuron*. 2008; 60(4):543–554.
44. van der Stelt M, Di Marzo V. The endocannabinoid system in the basal ganglia and in the mesolimbic reward system: implications for neurological and psychiatric disorders. *Eur J Pharmacol*. 2003; 480(1–3):133–150.
45. Shen W, Flajolet M, Greengard P, Surmeier DJ. Dichotomous dopaminergic control of striatal synaptic plasticity. *Science*. 2008;321(5890):848–851.
46. Kreitzer AC, Malenka RC. Endocannabinoid-mediated rescue of striatal LTD and motor deficits in Parkinson's disease models. *Nature*. 2007; 445(7128):643–647.
47. Maher PA, Singer SJ. Anomalous interaction of the acetylcholine receptor protein with the nonionic detergent Triton X-114. *Proc Natl Acad Sci U S A*. 1985;82(4):958–962.
48. Wetterhall M, Shevchenko G, Artemenko K, Sjodin MO, Bergquist J. Analysis of membrane and hydrophilic proteins simultaneously derived from the mouse brain using cloud-point extraction. *Anal Bioanal Chem*. 2011;400(9):2827–2836.
49. Page ME, Brown K, Lucki I. Simultaneous analyses of the neurochemical and behavioral effects of the norepinephrine reuptake inhibitor reboxetine in a rat model of antidepressant action. *Psychopharmacology (Berl)*. 2003;165(2):194–201.
50. Sulzer D, Edwards R. Vesicles: equal in neurotransmitter concentration but not in volume. *Neuron*. 2000;28(1):5–7.
51. Goldberg MS, et al. Nigrostriatal dopaminergic deficits and hypokinesia caused by inactivation of the familial Parkinsonism-linked gene DJ-1. *Neuron*. 2005;45(4):489–496.
52. Richter A, Loscher W. Pathology of idiopathic dystonia: findings from genetic animal models. *Prog Neurobiol*. 1998;54(6):633–677.
53. Wang JQ, McGinty JF. The full D1 dopamine receptor agonist SKF-82958 induces neuropeptide mRNA in the normosensitive striatum of rats: regulation of D1/D2 interactions by muscarinic receptors. *J Pharmacol Exp Ther*. 1997;281(2):972–982.

Dopamine dysregulation in a mouse model of paroxysmal non-kinesigenic dyskinesia

Hsien-yang Lee, Junko Nakayama, Ying Xu, Xueliang Fan, Maha Karouani, Yiguo Shen, Emmanuel N. Pothos, Ellen J. Hess, Ying-Hui Fu, Robert H. Edwards and Louis J. Ptáček

Supplemental Figure 1

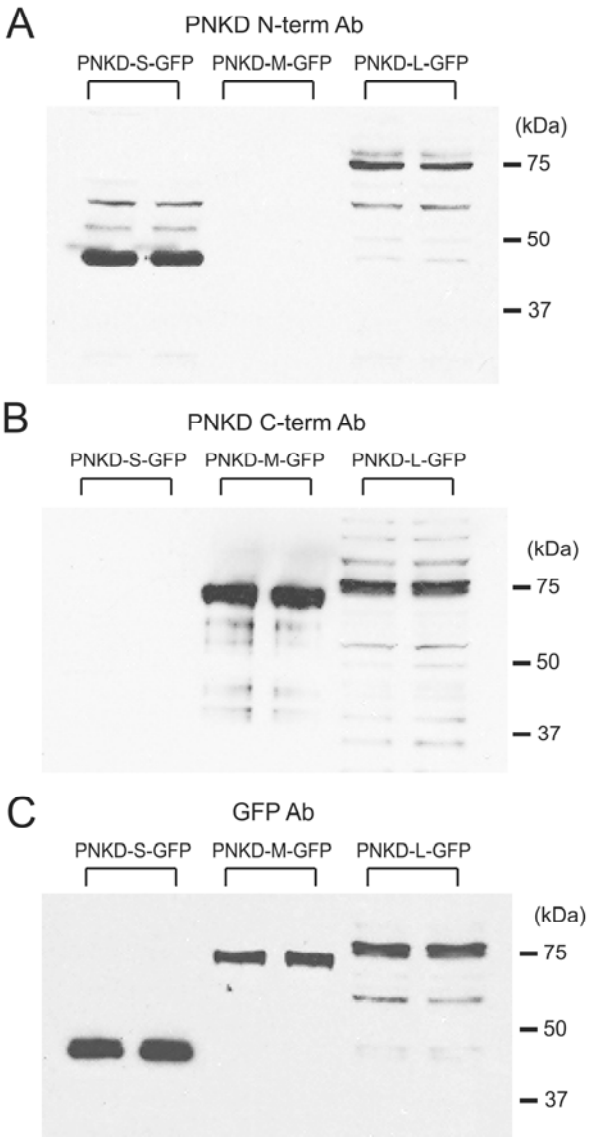

Supplemental Figure 1

Western blot analyses of HEK293 cell extractions transfected with different isoforms of *PNKD-EGFP* by using PNKD antibodies and GFP antibody. PNKD N-terminal antibody can detect both PNKD-L-EGFP (~75 kDa) and PNKD-S-EGFP (~44 kDa), and PNKD C-terminal antibody can detect both PNKD-L-EGFP and PNKD-M-EGFP (~70 kDa). GFP antibody can positively identify all three EGFP-fusion proteins at similar sizes compared with PNKD antibodies.

Supplemental Figure 2

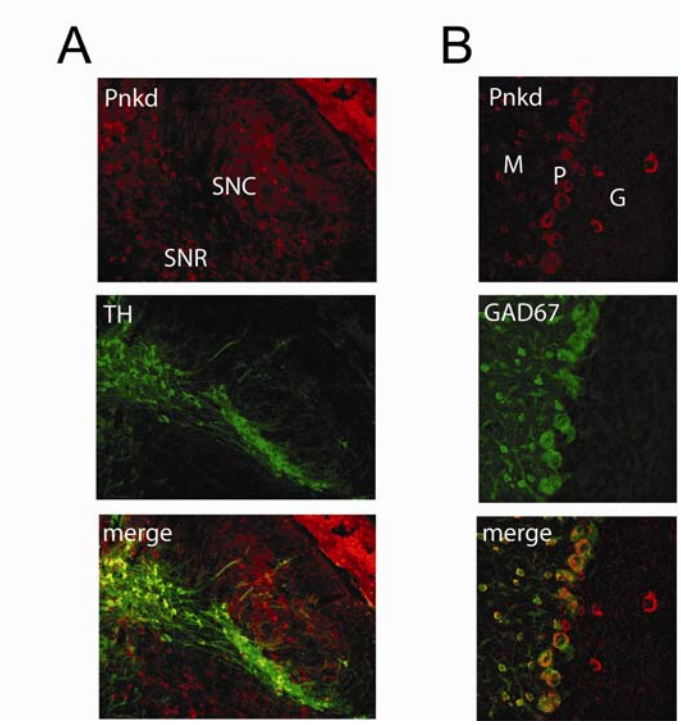

Supplemental Figure 2

Pnkd immunochemistry in mouse brain. **(A)** Pnkd is expressed in substantia nigra pars reticulata (SNR), and substantia nigra pars compacta (SNC). In SNC, Pnkd is co-localized with the dopaminergic neurons which are positive for tyrosine hydroxylase (TH). Original magnification, x400. **(B)** In cerebellum, Pnkd is widely expressed in the Purkinje cells, and the molecular and granule cell layers. Purkinje cells and neurons in the molecular layer are co-labeled with anti-glutamate decarboxylase 67 (GAD67). Original magnification, x630.

Supplemental Figure 3

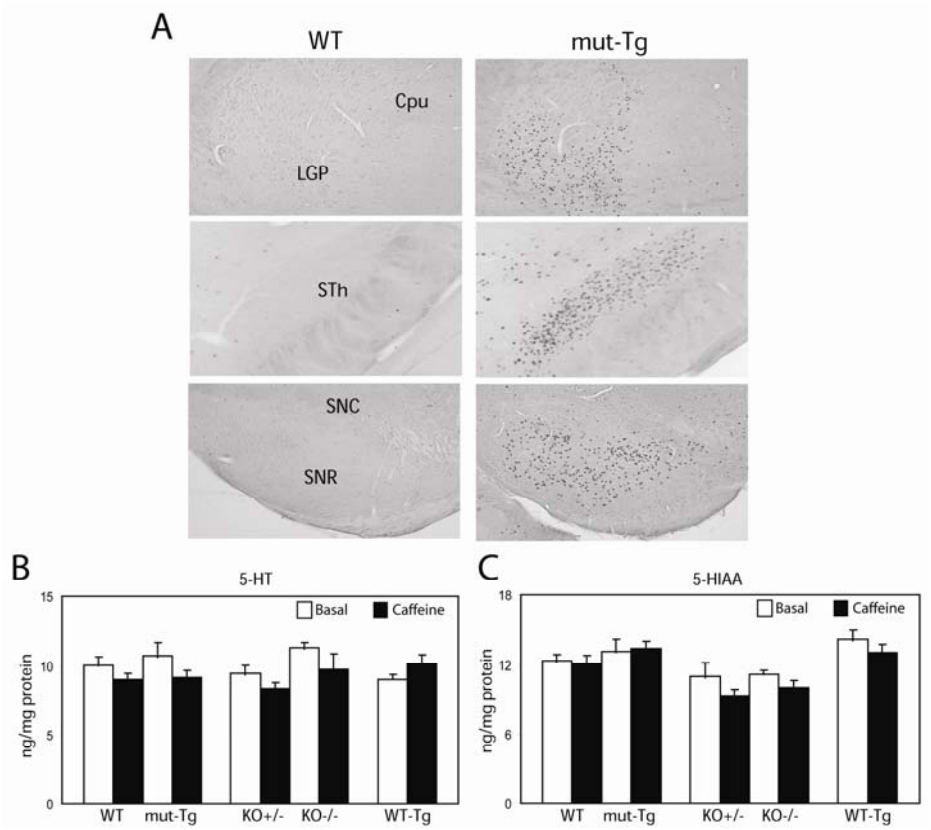

Supplemental Figure 3

After caffeine treatment, strong c-Fos staining is detected in the basal ganglia of Pnkd (mut-Tg) mice vs. WT littermates but no obvious differences in 5-HT signaling pathways of PNKD mice or WT littermates were seen. **(A)** c-Fos immunohistochemistry in basal ganglia of Pnkd mice and WT littermates 2 hours after caffeine stimulation. Strong induction of c-Fos was detected in the lateral globus pallidus, subthalamic nucleus, and substantia nigra pars reticulata of Pnkd mice, but not in WT littermates. Abbreviations: **Cpu**, caudate putamen; **LGP**, lateral globus pallidus; **STh**, subthalamic nucleus; **SNR**, substantia nigra pars reticulata. Original magnification, x50. **(B, C)** There were no changes in the levels of serotonin (5-HT) or 5-hydroxyindoleacetic acid after caffeine treatment. All data are presented as mean ± SEM (n=10-12 mice for each group).

Supplemental Figure 4

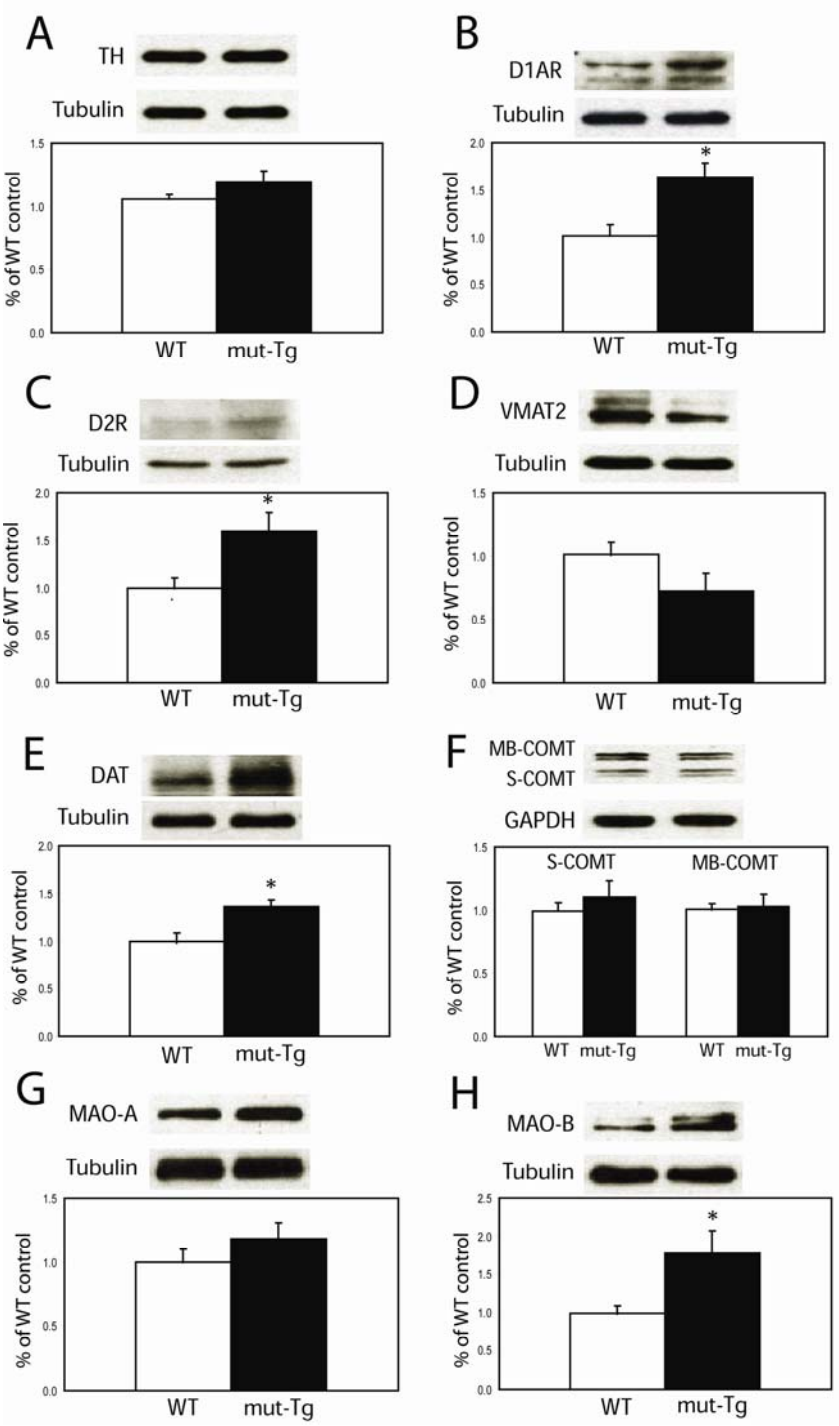

Supplemental Figure 4

Western analysis shows no differences between Pnkd (mut-Tg) mice and WT littermates for a number of dopamine signaling and metabolism proteins, but the dopamine receptor, dopamine transporter, and monoamine oxidase B proteins are up-regulated in Pnkd mice. **(A)** No difference was found between genotypes for the expression levels of tyrosine hydroxylase (TH) in striatum of Pnkd mice and WT controls. **(B)** The protein levels of dopamine D_{1A} receptor (D1AR) is significantly higher in Pnkd mice compared with WT littermates ($P<0.05$). **(C)** The protein levels of dopamine D_2 receptor (D2R) is up-regulated in Pnkd mice compared with WT littermates ($P<0.05$) **(D)** The protein levels of vesicular monoamine transporter 2 (VMAT2) trended to being decreased in Pnkd mice vs. controls but the difference was not statistically significant. **(E)** The protein levels of dopamine transporter (DAT) is significantly higher in Pnkd mice compared with WT littermates ($P<0.05$). **(F, G, H)** There were no obvious differences in expression levels of two isoforms of catechol o-methyltransferase (COMT) and monoamine oxidase A (MAO-A) between genotypes, but the amount of monoamine oxidase B (MAO-B) is significantly increased in Pnkd mice ($P<0.05$). All data are given as mean ± SEM ($n = 8$ for each genotype).

Supplemental Figure 5

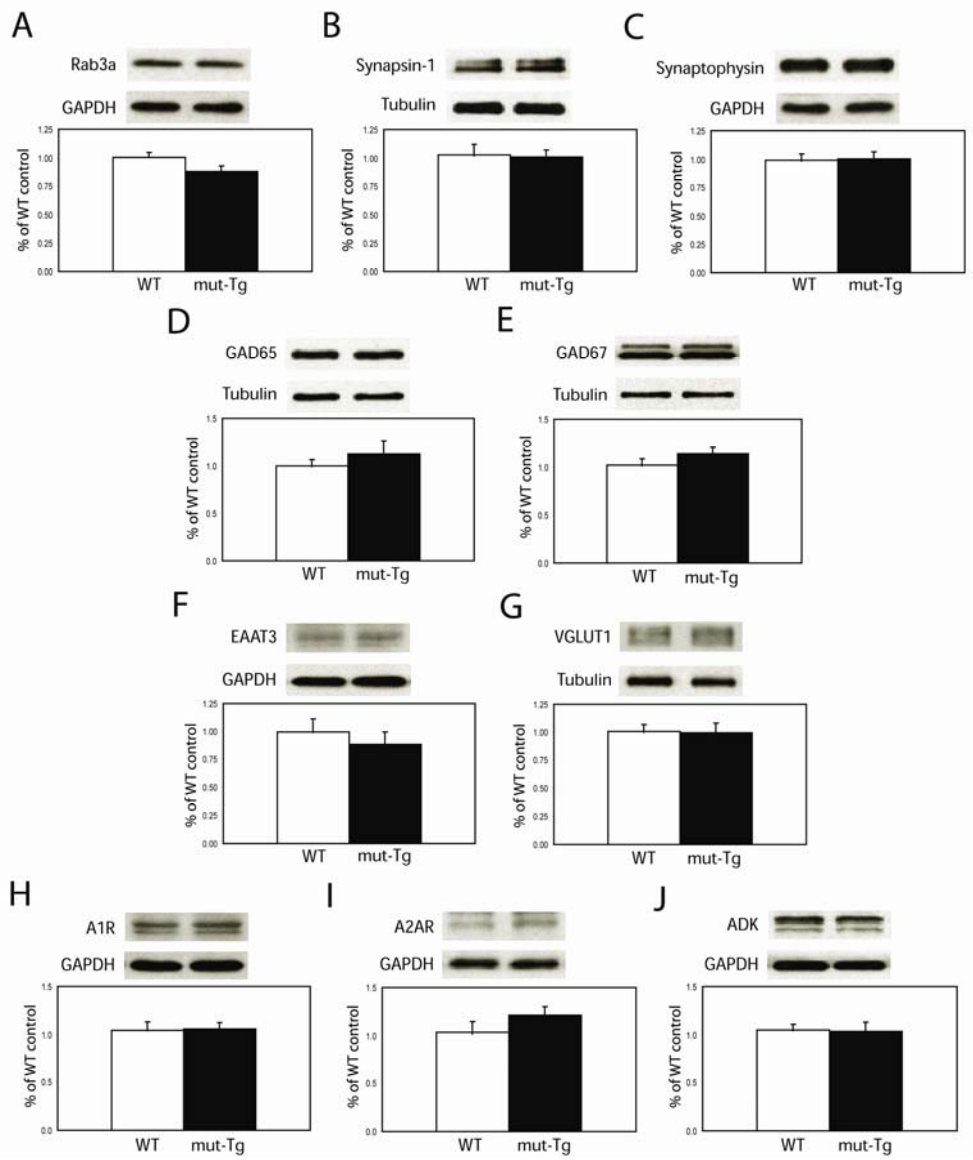

Supplemental Figure 5

Western analysis shows no differences between Pnkd (mut-Tg) mice and WT littermates for a number of striatal proteins. There were no differences in expression levels of **(A)** Rab3a, **(B)** synapsin-1, and **(C)** synaptophysin, **(D, E)** glutamate decarboxylase 65 and 67 (GAD65 and GAD67), **(F)** There were no differences in expression levels of excitatory amino acid transporter 3 (EAAT3), **(G)** vesicular glutamate transporter (VGLUT1), **(H, I)** adenosine A_1 and receptors (A_1R, $A_{2A}R$), and

(J) adenosine kinase (ADK) in mutant vs. control animals. All data are given as mean ± SEM (n = 8 for each genotype).

Supplemental Figure 6

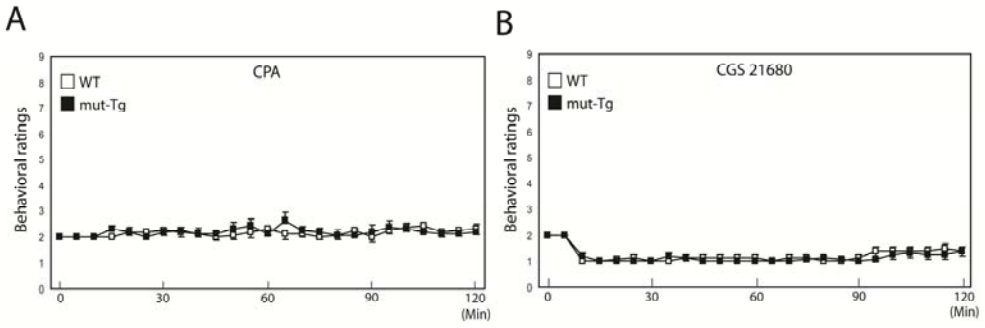

Supplemental Figure 6

A_{1A} and A_2 Receptor Neuropharmacology. **(A)** No difference in activity ratings of Pnkd mice (mut-Tg) and WT littermates (WT) were observed after adenosine A_1 receptor agonist CPA (0.1 mg/kg, IP) or **(B)** adenosine A_2 receptor agonist CGS21680 (0.5 mg/kg, IP). Reduced activity was observed after treatment with CGS 21680, but no obvious difference is found between genotypes. These behavioral ratings are expressed as mean ± SEM (n = 8 for each group).

Figure legends of supplemental videos

Supplemental video 1.

Stress induced dyskinetic attacks in Pnkd mouse. In Pnkd (mut-Tg) mouse, stress by prolonged handling (>15-30 minutes) induced dyskinetic attacks.

Supplemental video 2.

Caffeine induced dyskinetic attacks in Pnkd mouse. In Pnkd (mut-Tg) mouse, caffeine (25 mg/kg) induced dyskinetic attacks ~15-20 minutes after treatment.

Supplemental video 3.

Ethanol induced dyskinetic attacks in Pnkd mouse. Ethanol (1.5 g/kg, 20% v/v) also induced dyskinetic attacks in the Pnkd (mut-Tg) mouse (right side) but not in WT littermate (left side) after **(A)** 15 minutes, and **(B)** 1 hour of injection.

Supplementary Methods

PNKD Antibodies. Polyclonal antibodies were developed (Covance, Berkeley, CA) using two synthesized oligopeptides corresponding to the N-terminus of PNKD-L and S (MAAVVAATALKGRGARNARVLRGC), and the C-terminus of PNKD-L and M (CDDYSRAQLLEELRRLKDMHKSK). Pre-immune bleeds and test bleeds were obtained individually from the supplier to monitor antibody titer and specificity in subsequent bleeds. Antibodies were affinity-purified using the oligopeptides coupled to activated CH-Sepharose 4B beads (Amersham Biosciences, Piscataway, NJ). Antisera were added to the bead preparations, rotated, and incubated overnight at 4°C. Antiserum/bead mixtures were then poured into a 10 mL Poly-prep chromatography column (Bio-Rad, Hercules, CA), washed with four bead volumes of 1X phosphate-buffered saline (PBS) without calcium and magnesium (Gibco, Carlbad, CA), and eluted with 40 X 500μL fractions of 100mM glycine (pH 2.7) into microcentrifuge tubes containing 300μL 200mM Na_2HPO_4. Absorbance at 280nm was determined using the Coomassie PlusProteinAssay kit (Pierce Biotechnology, Rockford, IL) for each fraction with a DU 530 UV/Vis spectrophotometer (Beckman Coulter, Fullerton, CA). Affinity-purified antibodies were then used for Western blotting and immunohistochemistry experiments.

Generation of Pnkd transgenic mice. RP24-112K19 is a bacterial artificial chromosome (BAC) clone from the RP-24 mouse genomic library containing the entire *Pnkd* locus on a 183-kb genomic insert with 62kb upstream of the gene (Children's Hospital Oakland Research Institute). We constructed a rpsl/kan counter selection fragment. The primers were designed with 20 nucleotides for amplification of the rpsl/kan gene and an additional 50 nucleotides homologous to sequences flanking the region corresponding to the mutant region. This PCR product was transferred into the RP24-112K19 BAC by homologous recombination in *E. coli* strain DH10B already containing the plasmid pKD46 (1). The counter selection gene was removed by recombination using a synthetic oligonucleotide in the position carrying the Ala7Val and Ala9Val mutations as described elsewhere with modification (2). ET-cloning was then employed to introduce an internal ribosome entry site (IRES) followed by an enhanced red fluorescent protein gene (IRES/DsRed) into the 3' UTR of the *Pnkd* gene. All relevant segments generated by PCR and recombination were sequence confirmed. Purified BAC DNA (Nucleobond, BD) was subjected to Southern blotting to confirm correct homologous recombination. BAC DNA was digested with NotI restriction enzyme, run on a pulse field gel to identify the best samples to inject, and concentration of BAC DNA without linearization for injection

was adjusted to 1 ng/μL with microinjection buffer. WT transgenic mice were generated by microinjecting an unmodified BAC clone. The transgenic founders had a mixed C57BL/6XSJL F1 background and were backcrossed to C57/BL6 for >10 generations.

Generation of Pnkd knockout mice. To generate the targeting vector, a 2.6 kb short homologous arm upstream of *Pnkd* exon 5, was amplified with the LA PCR kit (Takara, Japan) using primers 5'-GCCCGGGCAGAAAGAGAGCGAAGTCAGAGAAG-3' and 5'-CTCGAGGAGCTCAGTACTGTCTGTAGGCCTCACATCTCTAGG-3'. A 6.5 kb long homologous arm, which is down stream of exon 9 was amplified using primers 5' CTCGAGGTGGTGAGTTTCTGCAAAAGAGAG-3' and 5'-ATCAGGTTTCCATGGTTTTGCTAT-3'. The fragments were inserted separately into the pMCIDT-A PGKNeo vector. About 1.5kb of genomic DNA, including exons 5 to 9, was replaced by the neomycin resistance gene. The targeting vector was linearized with *Not*I and used for electroporation into embryonic stem (ES) R1 cells. Culture of ES cells and isolation of homologous recombinants were performed according to standard protocols. Briefly, 10^7 R1 ES cells were transfected with 25 to 50 μg of the linearized vector. Cells were cultured under selection in G418. Resistant colonies were expanded in 96-well plates. Screening for homologous recombinants by PCR used amplification of external short arm area primer 5'-AGAGGCCACAGAAGGGAAGT-3' and vector side 5'GCCTCACATCTCTAGGATCTCTGT-3', and vector side 5'-GTTCTTCTGAGGGGATCAATTCTCTA-3' and external long arm area 5'-GATCCTTATAGGTCAAAGAGCAGGAG-3'. Positive ES clones were injected into C57BL/6J blastocysts and implanted in pseudopregnant females. Chimeric mice were screened using PCR and Southern blotting to detect recombinants and mated with C57BL/6 mice to produce F_1 heterozygous mice and heterozygotes identified by PCR. Confirmed *Pnkd* +/- F_1 mice were backcrossed to C57BL/6J mice or mated with siblings to generate null mutant mice.

Genotyping. PCR was performed on genomic DNA isolated from tail cuts of *Pnkd* transgenic, KO, and WT mice. PCR was performed using the following primer sets: 5'-TAGCGCTACCGGACTCAGAT-3' and 5'-AGGAACTGCTTCCTTCACGA-3' (mutant transgenic), 5'-AGTGCAGTCGTAAAAGTCAGAAC-3' and 5'-ACATACATGCAGGAAAACAACCA-3' (WT transgenic), and 5'-AGGATCTCCTGTCATCTCACCTTGCTCCTG-3' and 5'-AAGAACTCGTCAAGAAGGCGATAGAAGGCG-3' (KO mice). PCR was for 3 minutes at 94°C, 35 cycles of amplification (30s at 94°C, 30s at 60°C, and 60s at 72°C), followed by 3 minutes final extension at 72°C.

Immunoblotting. For Western blotting tissue homogenates obtained from *Pnkd* WT, transgenic and KO mice, protein concentrations were determined using a protein assay kit (Pierce, Rockhold, IL). Brain homogenates containing 20μg of protein were resolved on 10% polyacrylamide gels and electroblotted to nitrocellulose membrane using 50mM Tris-HCl buffer (pH 8.4). The blot was incubated with anti-PNKD antibody for 1 hour and detected using an ECL western blot chemiluminescent kit (GE Healthcare, Buckinghamshire, UK). Blots were stripped and reprobed with an anti-α-tubulin antibody (1:5000; Sigma, St. Louis, MO). Densitometry was performed using a Kodak 1-D system (Eastman Kodak, Rochester, NY). Pnkd levels were normalized to α-tubulin using the average pixel intensity for immunoreactive band in each lane and the images were analyzed by the NIH ImageJ software.

For the comparison of the levels of different proteins in striata of Pnkd mice and WT littermates, the dorsal striata of mice (n=8/genotype) were dissected and snap frozen in liquid nitrogen. Striata were sonicated in 300 μl of RIPA buffer (10mM Tris-HCl pH 7.2, 150mM NaCl, 5mM EDTA, 1% Triton X-100, 1% SDS, 1% Deoxycholate) with protease inhibitor (Roche, Mannheim, Germany) and phosphatase inhibitor cocktails (Sigma, St. Louis, MO). Equal amounts of protein from the total striatal homogenate were used for the Western blot analysis as described above. Blots were then incubated with one of the following antibodies in 1:1000 dilution: anti-vesicular glutamate transporter 1 (VGLUT1), anti-Rab3A and anti-synaptophysin (Synaptic Systems, Goettingen, Germany); anti-excitatory amino acid transporter 3 (EAAT3), anti-monoamine oxidase A (MAO-A), and anti-monoamine oxidase B (MAO-B) (Santa Cruz biotechnology, Santa Cruz, CA); anti-adenosine kinase (ADK) (Abcam, Cambirdge, MA); anti-adenosine A_1 receptor (A_1R, EMD, Darmatadt, Germany); anti-catechol o-methyltransferase (COMT, BD biosciences, San Jose, CA); anti-synapsin-1, anti-glutamate decarboxylase 65 (GAD65), anti-glutamate decarboxylase 67 (GAD67), anti-adenosine A_{2A} receptor (A_{2A}R), anti-tyrosine hydroxylase (TH), anti-dopamine transporter (DAT), anti-dopamine D_{1A} receptor (D_{1A}R), anti-dopamine D_2 receptor (D_2R), and anti-vesicular monoamine transporter 2 (VMAT2) (Millipore, Billerica, MA), Detected was performed as described above, and were stripped and reprobed with either anti-α-tubulin or anti-glyceraldehyde 3-phosphate dehydrogenase (GAPDH) antibody (Millipore, Billerica, MA). Striata protein levels were normalized and data were analyzed using Student's *t* test.

RT-PCR. Total RNA was extracted from mouse brain with TRIzol (Invitrogen) according to the manufacturer's instructions, and then subjected to DNase treatment (Ambion). RNA (10μg) was reverse-transcribed using Superscript III (Invitrogen). The primer sequence for *Pnkd* were 5'-TGCTATTCTTCGCCTTCGTGCTG-3' and 5'-CCTGGCCCCAGAGCCTCCTGTAGT-3' (*Pnkd-M*), and

5’-GGGGTGGGACCCGAACATGGCGGC-3’ and 5’-CCTGGCCCCAGAGCCTCCTGTAGT-3’ (*Pnkd-L*). The following conditions were used for PCR: 3 minutes at 94°C, 35 cycles of amplification (30s at 94°C, 30s at 55°C, and 60s at 72°C), followed by 3 minutes final extension at 72°C.

Pnkd Immunohistochemistry in mice brain slides. Adult WT, and transgenic male mice were sacrificed, perfused, and brains/spinal cords were removed, fixed, postfixed, cryoprotected, and coronal sections were cut at 14 µm with a Leica CM1850 cryostat (Leica, Nussloch, Germany) and thaw-mounted onto Superfrost Plus slides (Fisher, Pittsburgh, PA). The sections were washed in 1 X PBST (PBS with 0.3% Triton X-100) for 5 minutes, then blocked by 10% normal goat serum-PBST (NGS-T) for 1 hour. Fluorescence immunohistochemistry staining was performed by incubating overnight in 2% NGS-T with PNKD N-terminal antibody (1:250 to 1:500 diluted) or PNKD C-terminal antibody (1:5000 diluted), and co-labeled with mouse monoclonal antibodies for detection of either neuron-specific nuclear protein (NeuN), glial fibrillary acidic protein (GFAP), myelin basic protein (MBP), dopamine- and cyclic AMP-regulated neuronal phosphoprotein with molecular weight 32 kDa (DARPP-32), choline acetyltransferase (ChAT), parvalbumin, glutamic acid decarboxylase isoform 67 (GAD67), or tyrosine hydroxylase (TH) (Chemicon, Temecula, CA). After three washes with 2% NGS-T, sections were then incubated in 2% NGS-T with Cy^{TM}3-conjugated goat-anti rabbit IgG (diluted 1:300), alone or combined with Cy^{TM}2-conjugated goat-anti mouse IgG (1:50) (Jackson ImmunoResearch, West Grove, PA) for 1 hour, followed by washing three times in 1 X PBS-T in darkness. The sections were mounted under cover slides with Vectashield mounting medium (Vector Laboratories Inc. Burlingame, CA). Images were captured with a Zeiss Pascal LSM5 confocal microscope in the UCSF microscopy core and were imported into Photoshop (Adobe Systems, San Jose, CA) for analysis.

Immunostaining of transfected cells for PNKD-L localization. Human embryonic kidney (HEK)-293 cells were grown in Dulbecco’s modified Eagle’s medium (DMEM) supplemented with penicillin, streptomycin, and 10% fetal bovine serum (Hyclone, Logan, UT) and maintained at 37°C with 5% CO_2. After one day, the cells were split into 35mm culture dishes on coverslips pre-coated with poly-L-lysine (Sigma, St. Louis, MO). In parallel, HEK293 cells grown to 80-90% confluence were transfected with 2 µg DNA (*PNKD*-L, M, and S WT fusion constructs) using 20 µl of Polyfect reagent (Qiagen, Valencia, CA) using a standard protocol. Twelve hours post-transfection, cells were quick fixed in 4% paraformaldehyde and permeabilized with PBS/0.1% Triton or incubated in PBS and then stained with either PNKD N-terminal or C-terminal antibody followed by Cy^{TM}3-conjugated goat-anti rabbit

IgG (1:300) secondary antibody (Jackson ImmunoResearch, West Grove, PA) and mounted on Premium microscope slides (Fisher, Pittsburgh, PA) with Vectashield mounting medium (Vector, Burlingame, CA). Images were acquired using the Zeiss Pascal LSM5 confocal microscope in the UCSF microscopy core facility.

Mapping of c-Fos induction after a precipitation of a PNKD attack. Two hours after intraperitoneal (IP) injection of ethanol or caffeine, mice were perfused intracardially under deep tribromoethyl alcohol anesthesia with PBS followed by 4% paraformaldehyde in PBS. Following perfusion, brains were post-fixed and sliced into 30μM coronal sections using a vibratome. c-Fos immunohistochemistry was performed on free-floating brain slices. Brain sections were pretreated for 30 minutes 0.5 hour with 0.5% solution of H_2O_2 and blocked with 4% inactivated normal goat serum for 30 minutes in PBS/0.3% Triton X-100 prior to being rinsed with normal PBS. The primary antibody (Ab2, Oncogene Research Products) was diluted 1:1000 in PBS with 1% bovine serum alubumin (BSA)/0.3% Triton X-100 and incubated overnight at 4°C. Biotinylated goat anti-rabbit IgG (Oncogene Reseach Products) was diluted 1:400 in PBS with 1% BSA/0.3% Triton X-100. Sections were then incubated in avidin-biotin-horseradish peroxidase (Vectastain Elite ABC kit, Vector Laboratories Inc.) for 1 hour. Labeling was revealed by exposure to 3,3'-diaminobenzidine (DAB) substrate (Peroxidase Substrate kit, Vector Laboratories Inc.) for 10-15 minutes. The sections were then mounted under cover slides with Vectashield mounting medium (Vector Laboratories Inc. Burlingame, CA) and images were captured with a Nikon Eclipse microscope with a CCD camera or a Leica DM5000B microscope with a SPOT RT camera (SPOT diagnostic Inc., Sterling Heights, MI) and were imported into Photoshop program for analysis.

References

1. Datsenko, K.A., and Wanner, B.L. 2000. One-step inactivation of chromosomal genes in Escherichia coli K-12 using PCR products. *Proc Natl Acad Sci U S A* 97:6640-6645.
2. Narayanan, K., Williamson, R., Zhang, Y., Stewart, A.F., and Ioannou, P.A. 1999. Efficient and precise engineering of a 200 kb beta-globin human/bacterial artificial chromosome in E. coli DH10B using an inducible homologous recombination system. *Gene Ther* 6:442-447.